In presenting the dissertation as a partial fulfillment of the requirements for an advanced degree from the Georgia Institute of Technology, I agree that the Library of the Institute shall make it available for inspection and circulation in accordance with its regulations governing materials of this type. I agree that permission to copy from, or to publish from, this dissertation may be granted by the professor under whose direction it was written, or, in his absence, by the Dean of the Graduate Division when such copying or publication is solely for scholarly purposes and does not involve potential financial gain. It is understood that any copying from, or publication of, this dissertation which involves potential financial gain will not be allowed without written permission.

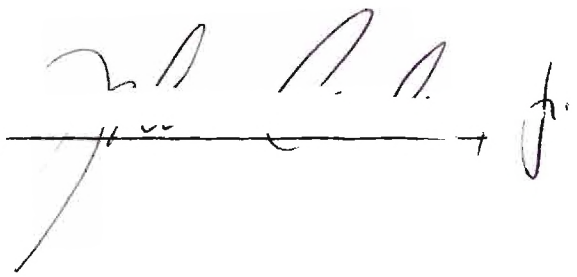

7/25/68

THE ADSORPTION OF KRYPTON ON THE (1,1,1) FACE OF COPPER

A DISSERTATION

Presented to

The Faculty of the Division of Graduate Studies and Research

By

John Lewis Carden, Jr.

In Partial Fulfillment

of the Requirements for the Degree

Doctor of Philosophy

in the School of Chemistry

Georgia Institute of Technology

June, 1972

THE ADSORPTION OF KRYPTON ON THE

(1,1,1) FACE OF COPPER

Approved:

Robert A. Pierotti, Chairman

Date approved by Chairman: 22 June 1972

ACKNOWLEDGMENTS

The author wishes to express his appreciation to all of those who aided him in the course of this study.

Special thanks are given to Dr. Robert A. Pierotti who suggested the problem, provided the funds necessary for its persuit, and offered advice and encouragement throughout the program. Also Drs. Howard Thomas, David Newsome, and Reginald Ramsey did much to enrich the study.

Thanks are extended to Messrs. Malcom Rucker and Donald Lillie for assistance in the construction of the apparatus.

Messrs. James House and Charles Wagner are thanked for their participation in the x-ray and Auger analyses of the copper sample.

Mesdames Caron Crane and Mary Haack are thanked for their diligent efforts in the preparation of the final manuscript.

Finally the author wishes to thank his wife Ayşe who not only endured the program but gave vital assistance on numerous occasions.

TABLE OF CONTENTS

LIST OF TABLES

LIST OF ILLUSTRATIONS

SUMMARY

Isotherms of krypton adsorbed on the (1,1,1) face of copper single crystals were measured at 78.86, 91.17, 98.64, and 107.96 degrees Kelvin. Surface coverages over the range $0.05 < \theta < 1.5$ were obtained.

The copper sample was composed of thin single crystal flats which were electropolished to produce a planar surface. The geometric area of the surface of the sample was 78.6 cm^2. One of the crystals was analyzed by Auger electron spectroscopy to determine the elemental composition of the first few atomic layers at the surface.

The apparatus constructed for this study consisted of an ultra-high vacuum volumetric adsorption apparatus and a high pressure boiling liquid cryostat. The equilibrium pressure measurements were made with a MKS Baratron capacitance manometer, and the temperature range accessible for study using liquid nitrogen as the cryogenic bath was $78 < T < 109^{\circ}K$.

The data were analyzed with the virial and significant structures theories. A straight forward application of the virial equation of state did not fit the low coverage behavior of the isotherms, consequently the parameters obtained from the treatment could not be interpreted with certainty. The significant structures theory did fit the isotherms well and the treatment gave values of 3490 cal/mole for $\epsilon^*_{1,S}$, the minimum in the copper-krypton potential, and 95 cal/mole for $\epsilon^*_{1,2}$, the minimum in the krypton-krypton potential in the presence of the copper surface. This value of $\epsilon^*_{1,2}$ indicates that the krypton-krypton potential is reduced

by 70 percent as the pair of interacting atoms moves from isolation in the gas phase to the vicinity of the copper interface.

CHAPTER I

INTRODUCTION

Physical Adsorption

The study reported here involved a phenomenon generally referred to as physical adsorption. We shall begin then with a brief discussion of this phenomenon.

The following experiment might be considered one of many possible operational definitions of adsorption. Consider a container into which a solid with a large surface area (the adsorbent) has been placed. Let the unoccupied volume of the container be V. Now suppose that a quantity (N_d) of gas (the adsorbate) with a known equation of state is expanded into the container. When equilibrium has obtained at a temperature T the gas will exert a pressure P_e. If the values of P_e, V, and T, are now substituted into the equation of state of the gas, the apparent amount N_v of gas present in the container may be calculated. It is generally found that N_d and N_v are not equal, and the quantity $N_a = N_d - N_v$ is referred to as the amount of gas adsorbed. If the temperature is held constant and additional known quantities of gas are added or removed from the container, a curve may be constructed from pairs of corresponding N_a and P_e values. Such N_a versus P_e curves at constant temperature are referred to as isotherms, and the pairs of N_a and P_e values are called points. If a family of isotherms is collected over some temperature range, all of the thermodynamic properties of the adsorption system may

be calculated for that range. Also statistical and quantum mechanical considerations indicate that much information about the forces acting in the adsorption system may be obtained from the temperature dependence of the adsorption phenomenon.

The experiment described above is an example of what is known as gas-solid adsorption, and is similar to the work to be discussed here. Adsorption, however, is a phenomenon which is associated with interfaces in general whether it be between two liquids, a liquid and a gas, a liquid and a solid, or a solid and a gas.

The adsorption process is generally rationalized in the following way. Quantum mechanical calculations indicate[1] that when an adsorbate atom approaches the surface of the adsorbent, interactions take place which alter the potential energy of the adsorbate. These interactions are attractive and the adsorbate atom moves toward the surface thereby reducing its potential energy. As the atom comes near the surface a repulsive force grows in importance and at some distance z^* above the surface, the potential of the adsorbed atom goes through a minimum and then increases rapidly. Figure 1 illustrates the dependence of the potential energy of the adsorbate on its distance (z) from the interface. The effect of this potential gradient is the introduction of a density gradient into the adsorbate. The variation in the density of the adsorbate, due to the gas-solid interactions, relative to its density far from the interface is illustrated in Figure 2. In Figure 2A the minimum in the potential is one-half the kinetic energy of the adsorbate and in Figure 2B it is 10 times the kinetic energy.

If such a potential gradient is responsible for the observed

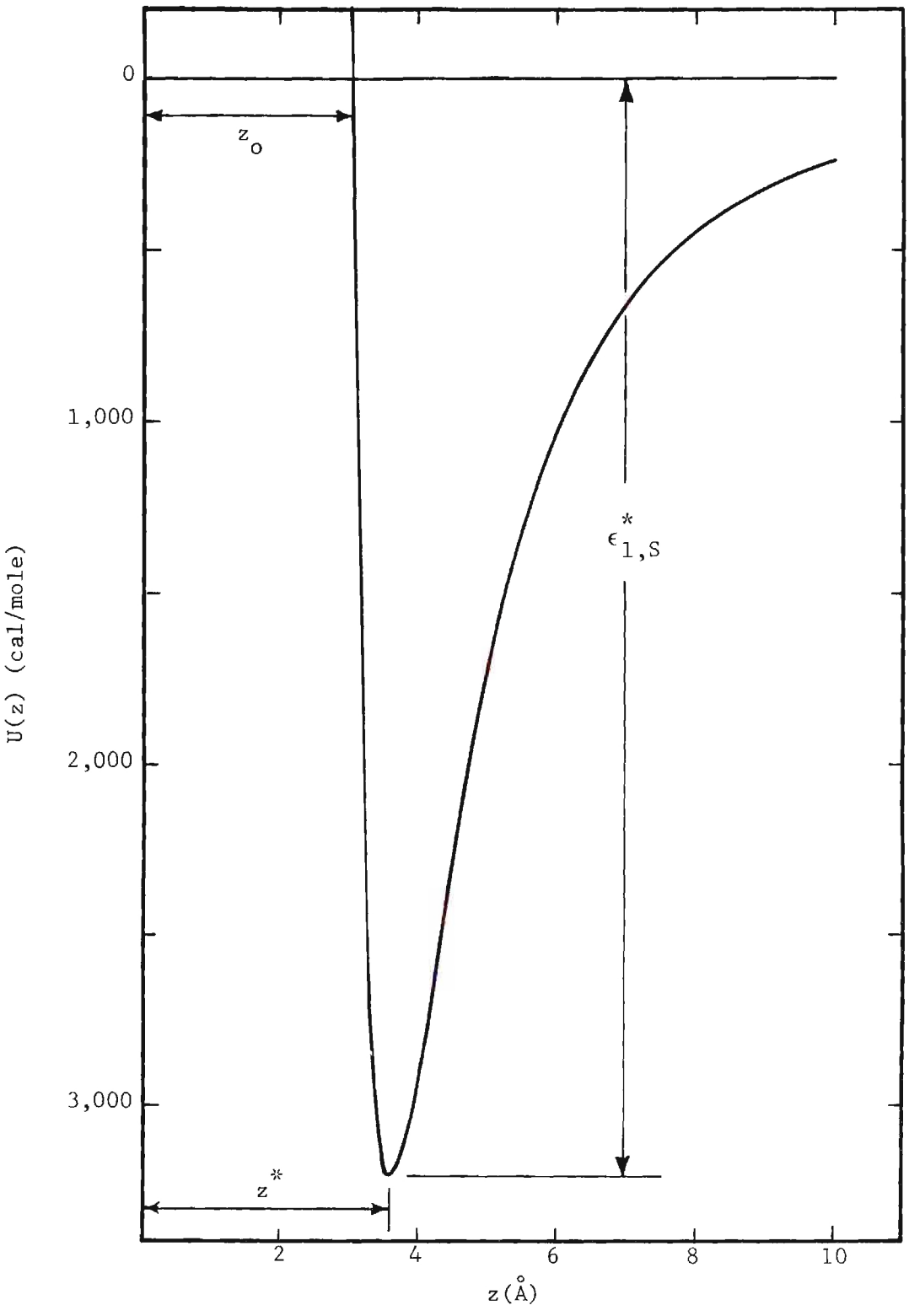

Figure 1. The Potential of an Atom Near an Interface

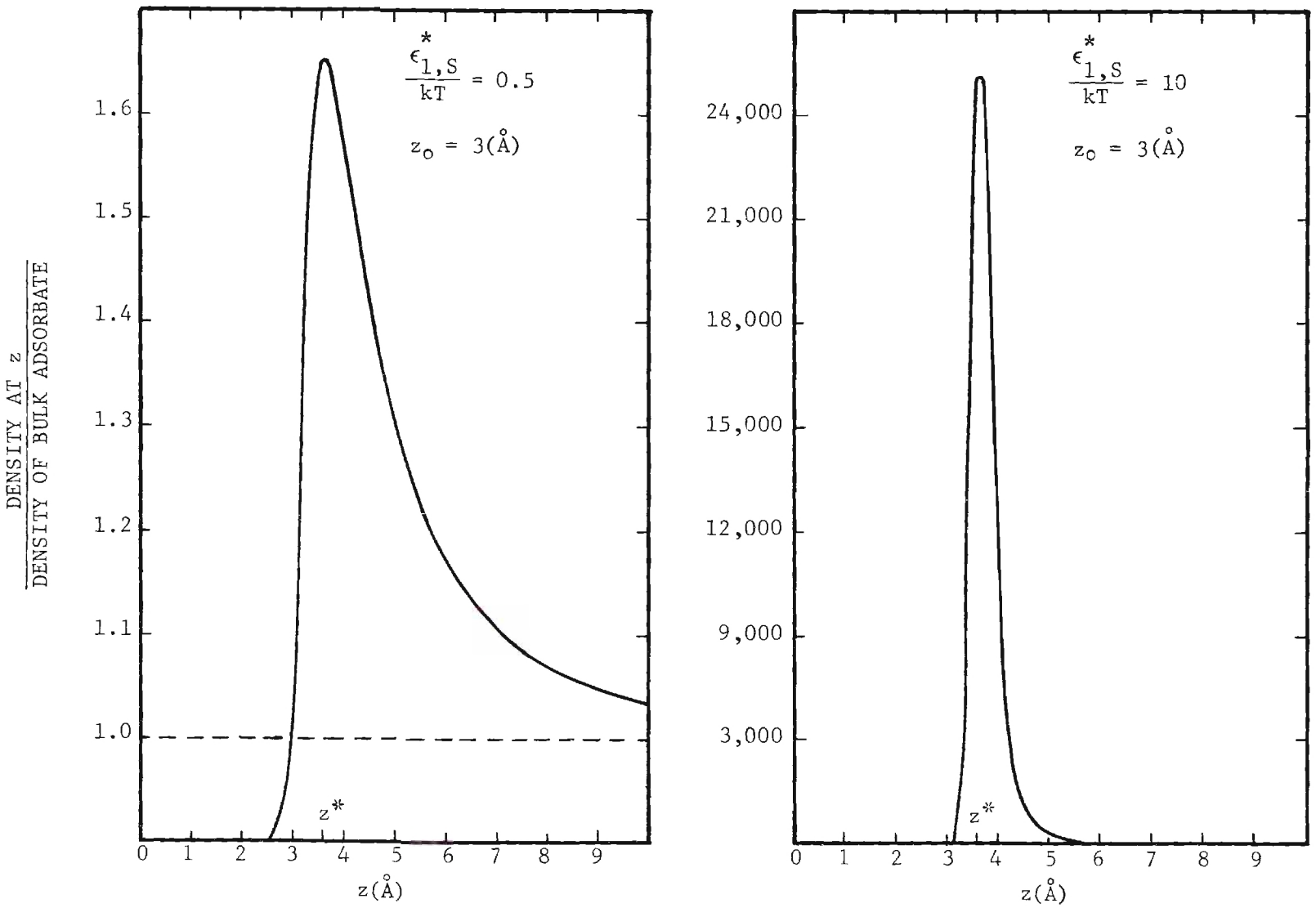

Figure 2. The Reduced Density of the Adsorbate Near an Interface

adsorption, the process is called physical adsorption. The heat associated with this process is of the order of the heat of vaporization of the bulk adsorbate. It is also possible in some systems (e.g., oxygen and solid aluminum) for the adsorbate atoms near the surface to react chemically with the atoms comprising the surface. This type of adsorption, which involves forces associated with an exchange of electrons, is called chemical adsorption or chemisorption.

At low temperatures, i.e., $\frac{\epsilon^*}{kT}$ is large, a film of adsorbate atoms may be formed on the adsorbent. If this film is one adsorbate atom thick and covers the entire surface, the film is called a monolayer. Additional layers may form and these are called the second layer, third layer, etc., or generally referred to as multilayers. This process of stepwise layer formation can continue until it is indistinguishable from condensation. The notion of the stepwise formation of monolayers and multilayers is, however, an idealization which is useful for discussion but unlikely to occur in real physical adsorption systems. For example, the second layer may be significantly filled before the first is completed.[2]

One final concept which must be mentioned is the surface area of the adsorbent. The knowledge of the surface area of a solid is often of great practical importance and much effort has been expended in attempting to develop improved methods for its determination. Ideally, the surface area of a solid might be defined as the geometric area of the interface between the solid and a vacuum; however, it is generally observed that the surface area indicated by adsorption measurements varies with the adsorbate and temperature, as well as with the model and assumptions chosen in order to extract the area from the data.[3]

Physical adsorption has been treated in many ways and the literature has been reviewed extensively (Brunauer,[4] Halsey,[5] Hill,[6] Steele,[7] Young and Crowell,[1] Flood[8]). The latest review was given by Pierotti and Thomas.[9]

The Forces Involved in Physical Adsorption

Physical adsorption has received much theoretical attention because it involves forces common to all dense phases but in a somewhat simpler context. The discussion to follow will indicate how certain aspects of these forces can be singled out for study by investigating specific regions of adsorption isotherms. Reviews of the literature concerned with forces in physical adsorption have been given by Honig[10] and others.[1,9]

Atom-Atom Interactions

The simplest approach is to begin by considering how two isolated atoms interact. The attractive interactions between atoms of a gas at moderate densities were first considered by van der Waals. These attractive forces are now generally referred to by his name. It was believed that these forces were wholly electrostatic in nature and much work went into explaining them. Significant progress was made in 1930 when London[11] proposed the existence of dispersion forces. London argued that while non-polar molecules and atoms do not on the average possess a dipole moment, they could have an instantaneous moment because the motion of the electrons around the atomic core could result in non-spherical charge distributions. Further these instantaneous or fluctuating dipoles could polarize a neighboring atom thus forming another dipole with which

the first could interact. He called the forces resulting from this sympathetic dipolar interaction dispersion forces. It is important to realize that the dispersion contribution to the total force acting between two molecules with permanent dipole moments is often larger than the contribution from the permanent dipoles (e.g., HCl, NH_3).

Attractive forces can also arise from interactions between instantaneous electron distributions of higher order than dipole waves, i.e., quadrupole moments, etc. Interactions are also possible between dipoles and quadrupoles.

The attractive or dispersion energy $U(r)_{disp.}$ resulting from the interaction between two isolated atoms may be written[12]

$$U(r)_{disp.} = -\frac{C}{r^6} - \frac{C'}{r^8} - \frac{C''}{r^{10}} + \text{higher order terms} \qquad (1)$$

where

C = constant dependent on the dipole-dipole interactions

C' = constant dependent on the dipole-quadrupole interactions

C'' = constant dependent on the quadrupole-quadrupole interactions

r = distance between the centers of the interacting atoms.

The constant C depends on properties of the individual interacting atoms and has been extensively investigated by perturbational and variational techniques.[1] Following the perturbational approach C depends on the energy levels and oscillator strengths of the atoms involved. The most commonly used relation for calculating C was given by Müller.[13]

The constants C' and C'' are more difficult to obtain from properties of the interacting atoms. Kiselev, et al.[14] have, however, estimated that the C' term contributes about 10 percent and the C'' term about 1 percent to the total dispersion interaction of a number of gases with a graphitic surface. Although these terms are significant they will be neglected henceforth, because they cannot at present be obtained with a reasonable degree of certainty from either experimental data or theoretical considerations.

As the two interacting atoms come into closer proximity, another electrostatic force, resulting from electron overlap between the atoms, grows rapidly in importance and results in a net repulsion. This repulsive force is much more difficult to treat theoretically because the interactions cannot be considered on the basis of properties of the independent isolated atoms involved. In fact, the repulsive potential has only been calculated for interactions between pairs of simple atoms. In surface studies the most commonly used form of the repulsive potential is

$$U(r)_{rep.} = \frac{B}{r^{12}} \qquad (2)$$

where B is an empirical constant. This equation does not arise from theoretical considerations but does represent fairly well the few calculations available and has a mathematical simplicity which makes it very attractive.

Since B, C', and C'' cannot in general be calculated from atomic properties, they must be extracted from experimental data. Normally,

however, the C' and C'' terms are neglected and their effect is absorbed in the repulsive constant B and the attractive constant C.

The total interaction potential between two isolated atoms may be written

$$U(r) = -\frac{C}{r^6} + \frac{B}{r^{12}} \tag{3}$$

or

$$U(r) = -\epsilon^* \left[2\left(\frac{r^*}{r}\right)^6 - \left(\frac{r^*}{r}\right)^{12} \right] \tag{4}$$

where $-\epsilon^* = U(r^*)$ = the minimum value of the potential between the interacting atoms and

r^* = the distance between the atoms at which this minimum occurs.

This function is frequently used in surface studies and is known as the Lennard-Jones (6-12) potential. Many other pair potential functions have been proposed, but all of the more realistic of these as well as the Lennard-Jones function suffer from significant theoretical shortcomings. These functions combine an attractive term which is only applicable when perturbations of the interacting atoms are small and consequently the atoms are relatively far apart with a repulsive term which approximates the potential between two atoms which are strongly perturbed and close together.

Interactions Between Atoms and Solids

Nonmetallic Solids. The forces that act between an adsorbed atom

and a solid are of the same general nature as those that act between isolated pairs, triplets, etc., of atoms but additional complications arise.

A rigorous treatment of the gas-solid interactions would require that the wave functions of the system as a whole be known, or at least that the wave functions of the isolated gas atom and solid be known. Although some progress has been made in this direction,[15] a high degree of approximation is usually required.

Dispersion forces are pairwise additive, consequently, it is possible to arrive at the dispersion potential between an adsorbed atom and the solid by applying an equation such as

$$U(r)_{disp.} = - \sum_{\substack{\text{All atoms} \\ \text{in the solid}}} \frac{C}{r_{g,i}^{6}} \qquad (5)$$

where

C = a constant dependent on the dispersion interactions between an isolated pair of adsorbate and adsorbent atoms

$r_{g,i}$ = the distance between the adsorbed atom and the i^{th} atom of the solid.

While it is known that the repulsive forces are not pairwise additive, the assumption is often made that they are; consequently, the total potential for one adsorbed atom and the solid may be represented by an equation such as

$$U(r) = -\epsilon^* \sum_{\substack{\text{All atoms} \\ \text{in the solid}}} \left[2\left(\frac{r^*}{r_{g,i}}\right)^{6} - \left(\frac{r^*}{r_{g,i}}\right)^{12}\right]. \qquad (6)$$

The Lennard-Jones (6, 12) function was used here but by making the same assumptions other potential functions could have been applied.

Hill[16] has shown that the problem may be further simplified by assuming that the solid is a semi-infinite continuum, bounded by a plane surface, of uniform density equal to that of the solid. Equation (6) can then be integrated and the potential is given by

$$U(z) = \pi\rho r^{*3}\epsilon^{*}\left[-\frac{1}{3}\left(\frac{r^{*}}{z}\right)^{3} + \frac{1}{45}\left(\frac{r^{*}}{z}\right)^{9}\right] \qquad (7)$$

where

ρ = density of the solid (atoms/unit volume)

$-\epsilon^{*} = U(r^{*})$ = the depth of the potential minimum between an isolated pair of gas and solid atoms

r^{*} = distance between the isolated pair at the potential minimum

z = the perpendicular distance of the adsorbate atom from the surface.

Note that the forces involving the surface are of a longer range (i.e., fall off less rapidly with separation) than those between an isolated pair of atoms.

The integration method of arriving at the adsorption potential has always been considered inadequate. The structure of the surface in the vicinity of the adsorbed atom plays too significant a role to be neglected as is the case in Equation (7).

A more realistic calculation may be made by carrying out the summation indicated by Equation (6) over the 100 or so atoms in the solid

nearest the adsorbed atom and then integrating the dispersion potential over the remainder of the semi-infinite solid described above. The adsorption potential for a number of systems has been calculated using this model and compared with experiments. Two interesting results have been found:

(1) U(z) for any given point in the plane of the surface has the form of Equation (7). This indicates that a pair potential function of the form

$$U(z) = -\frac{C}{z^3} + \frac{B}{z^9} \tag{8}$$

does represent the gas-solid potential. If this function is expressed in terms of the more relevant variables $\epsilon^*_{1,S}$, the minimum in the gas-surface potential and z_o, the distance above the surface at which the potential is zero, the result is

$$U(z) = \frac{3}{2}(3)^{\frac{1}{2}} \epsilon^*_{1,S} \left[\left(\frac{z_o}{z}\right)^9 - \left(\frac{z_o}{z}\right)^3\right] . \tag{9}$$

This is the function plotted in Figure 1 with $\epsilon^*_{1,S}$ = 3,200 cal/mole and z_o = 3 Å, values of the parameters which approximate those of the copper-krypton system.

(2) $\epsilon^*_{1,S}$ and z^*, the distance of the potential minimum above the surface, were found to depend on the position of the adsorbed atom in the plane of the surface.

Orr[17] has calculated that the energy of the lowest vibrational

state of an argon atom adsorbed on a perfect KCl crystal increases by 360 cal/mole as the argon atom moves from the center of a lattice cell to directly above a Cl^- ion. He also gives relations which are useful for making calculations above the (1,0,0) face of any solid which has a cubic lattice. Young[18] has done the same for the (1,1,1) face.

Crowell and Young[19] have applied the summation-integration technique to argon interacting with the basal plane of graphite. They calculated a barrier to translation in the plane of the surface from one potential minimum to another of approximately 50 cal/mole.

Metallic Solids. The treatment of metallic adsorbents has proceeded along different lines. Because of the presence of the conducting electrons at the metallic interface, metals have generally been modelled as continua. Lennard-Jones[20] first calculated the adsorption potential above a metal by assuming that the surface electrons were perfectly polarizable. This image field model led to energies that were too high. A number of investigators then treated the metal as a continuous dielectric medium, and found that the resulting energies were more reasonable. Finally, McLachlan[21] has extended the continuous dielectric model using reaction field theory. While McLachlan's model is as yet of little quantitative value it may lead the way to a more fundamental understanding of the origin of the forces acting as the gas-surface interface.

All of the models of the gas-metal potential have two common features. First, the repulsive forces are neglected and second, the structure of the solid is not considered. The work of Rhodin[22] has indicated that the structure of the metal is significant and must be taken into account in a realistic model. Further research is needed to confirm

Rhodin's findings and to provide a test for models of gas-metal interactions as they develop.

Interactions Between Adsorbed Atoms

The energy associated with the interactions between two adsorbed atoms is usually an order of magnitude less than that associated with the interactions between an adsorbed atom and the adsorbent. Even so, this lateral interaction energy leads to the formation of monolayers and multilayers, two of the most interesting features of adsorption systems. The discussion here will be confined to the interactions between two adsorbed atoms and the solid.

Freeman[24] and de Boer[23] found that the potential function which characterized the interactions between two isolated adsorbate atoms was inadequate to describe the interaction between the atoms when they were adsorbed. The presence of the surface seemed to result in an additional long-range repulsive force which offset to some extent the attractive forces acting between the adsorbed atoms.

Lateral forces have been treated in two ways; in terms of perturbation theory after Sinanoğlu and Pitzer[25] and in terms of electrical images or reaction field theory after McLachlan.[21]

Sinanoğlu and Pitzer considered the system of two or more atoms interacting with each other at the surface of a solid. They found that the gas-surface interactions were not altered by the presence of other adsorbate atoms, but that the presence of the solid introduced an additional term in the expression for the potential between two atoms interacting with each other and the surface. They showed that this pair potential could be written

$$U(r) = -\epsilon^* \left[2 \left(\frac{r^*}{r}\right)^6 - \left(\frac{r^*}{r}\right)^{12} \right] + \tag{10}$$

$$[S(R)/r^3](1 - 3\cos^2\theta)$$

where S(R) is a function of the mean distance of the pair of atoms from the surface, θ is the angle formed by a line through the centers of the atoms and a normal to the surface, and ϵ^* and r^* are the gas phase values for the adsorbate. The important conclusions of this study were (a) the potential energy of the adsorbate due to lateral interactions could be found by summing over pairs of atoms provided a term was added to the potential to account for the perturbation due to the solid and (b) the solid caused the potential between a pair of adsorbed atoms to be more attractive if one atom was above the other and less attractive if both atoms were in the plane of the surface. They also concluded that S(R) should be largest for solids with permanent electrostatic fields at their surfaces.

McLachlan[21] has treated the dispersion forces associated with the gas-metal interface in terms of electrical images. The fluctuating dipoles which result from the quantum motions of the electrons in the adsorbate atom are treated as oscillating charges which emit or absorb radiation. This radiation is absorbed by the electrons at the metal's surface thus producing an image of the dipole and providing an exchange of momentum which accounts for the gas-surface dispersion interaction. Two adsorbed atoms can interact directly by absorbing and emitting radiation, but an additional potential arises from the interaction between

an adsorbed atom and the image of another adsorbed atom and visa versa. This additional potential has the same orientational dependence as that of Sinanoğlu and Pitzer (i.e., repulsive when the adsorbed atoms are side by side and attractive when one is above the other). Unfortunately, the theory has little quantitative value because it is difficult to apply to real systems.

Statistical Models of Physical Adsorption

The interpretation of thermodynamic data in terms of molecular parameters is most reasonably carried out by using statistical mechanics to develop models of the system under study. Many such models have been developed in the area of physical adsorption[8] and the object here was to choose from among them the ones which most accurately represent the copper-krypton system. The two models chosen for the interpretation of these data in terms of the forces acting in the system are based on the virial and significant structures theories. These models as well as the older BET theory, used for surface area determinations, will be discussed in the remainder of this chapter.

The Virial Theory

The historical and theoretical origins of the virial theory of imperfect gases have been reviewed by Mason and Spurling.[26] Halsey and his students pioneered in the application of virial type equations of state to the physical adsorption problem, and Pierotti and Thomas[9] have reviewed recent developments in this area.

A virial analysis of gas-solid interactions was first applied to adsorption measurements by Steele and Halsey.[27] These authors treated

the gas-solid interactions in terms of V_{ex}, the apparent increase in the volume of the adsorption system due to the attractive interactions between the adsorbent and adsorbate. A more general approach is to expand the amount of gas adsorbed (N_a) in a power series in the equilibrium pressure or fugacity of the single component adsorbate, i.e.,

$$N_a = \sum_{i\geq 1}^{\infty} B_{(i+1),S} \left(\frac{f}{kT}\right)^i \tag{11}$$

where the $B_{(i+1),S}$ are the gas-solid virial coefficients.

Hill[28] and numerous others have shown how these virial coefficients are related to the potentials of the forces in the adsorption system. Pierotti[29] has discussed these interactions in terms of the more general "potential of average force" of McMillon and Meyer.[30]

$B_{n,S}$ is related to the n particle configuration integral for the system, consequently, $B_{2,S}$ may be written as an explicit function of the interactions between one adsorbate atom and the solid, i.e.,

$$B_{2,S} = \int_V (e^{-U(\bar{r}_1)/kT} - 1)d\bar{r}_1 \tag{12}$$

where

V = the volume accessible to the adsorbate

$\bar{r}_1$ = a vector which gives the position of the adsorbate atom relative to a point on the surface of the adsorbent.

If the field above the surface is assumed uniform, the integration may be carried out over the components of $\bar{r}_1$ in the plane of the surface (x,y) to give A, the area of the adsorbent. This leaves only the integration over the z component of the potential, and if equation (9) is assumed for U(z) the integral may be solved analytically to give

$$B_{2,S} = Az_o \sum_{\tau=0}^{\infty} \frac{1}{(9\tau!)} \left[\frac{(3)^{3/2}}{2} \frac{\epsilon^*_{1,S}}{kT} \right]^{\frac{6\tau+1}{9}} \Gamma[(3\tau - 1)/9] \qquad (13)$$

where

z_o = distance above surface at which U(z) = 0

Γ = the gamma function

A = area of the adsorbent

$-\epsilon^*_{1,S}$ = $U(z^*)$ = minimum value of gas-solid potential

T = temperature of the system.

Experimental values of $B_{2,S}$ determined at a number of temperatures can be analyzed in terms of $\epsilon^*_{1,S}$ and the product Az_o by applying equation (13). The area A can also be extracted if z_o is available from some other source.[31]

$B_{3,S}$ can be written in terms of the configuration integral for two adsorbate atoms interacting with each other and the adsorbent simultaneously. This coefficient then contains information about the lateral interactions within the adsorbed phase, but the relationship is complex. If the adsorbed phase is considered a two-dimensional film, a much simpler

relationship can be developed based on the virial equation of state of an imperfect two-dimensional gas. This equation is usually applied to the adsorbed film in the following form:[32]

$$\frac{\phi A}{N_a kT} = 1 + B_{2,D}\left(\frac{N_a}{A}\right) + C_{2,D}\left(\frac{N_a}{A}\right)^2 + \ldots \qquad (14)$$

where $B_{2,D}$, $C_{2,D}$, etc., are the two-dimensional virial coefficients and ϕ is the spreading or two-dimensional pressure.

The second two-dimensional virial coefficient, $B_{2,D}$, is given by

$$-B_{2,D} = \int_A (e^{-U(r)/kT} - 1)dr \qquad (15)$$

where r = distance between interacting adsorbed atoms.

If U(r) is given by equation (4), then (15) may be integrated resulting in

$$-\frac{B_{2,D}}{\pi\sigma^2} = \sum_{\tau=0}^{\infty} (12\tau!)^{-1}\left(\frac{4\epsilon^*_{1,s}}{kT}\right)^{(3\tau+1)/6}\Gamma\left(\frac{3\tau-1}{6}\right) \qquad (16)$$

where $\sigma = r_o$ = separation at which the potential is zero.

$-\epsilon^*_{1,2}$ = U(r*) = the minimum value of the potential between two interacting adsorbed atoms.

An analytical solution of equation (15) is also possible if the Sinanoğlu-Pitzer potential is assumed for U(r). Values of $B_{2,D}$ at

various temperatures can be analyzed in terms of $\epsilon^*_{1,2}$ and $\pi\sigma^2$ using equation (16).

It is possible to relate the two-dimensional virial coefficients of equation (14) to the three-dimensional ones of equation (11), thus the two dimensional coefficients can be obtained from the usual volumetric adsorption measurements. The Gibbs isotherm equation can be written

$$d\phi = (N_a kT/A)d \ln P . \tag{17}$$

If it is assumed that the adsorbate vapor is ideal far from the surface, which is essentially the case for krypton in these experiments, equation (11) may be solved for the pressure and substituted into equation (17) to yield

$$\frac{\phi A}{N_a kT} = 1 - \left(\frac{B_{3,S}}{2B_{2,S}^2} \right) N_a - \ldots . \tag{18}$$

By equating terms in like powers of N_a between equations (14) and (18) one finds

$$\frac{B_{2,D}}{A} = - \frac{B_{3,S}}{2B_{2,S}^2} . \tag{19}$$

Finally, the effect of surface heterogeneity on the parameters resulting from a virial treatment is a matter which has received some attention. The surface area is a convenient and important parameter to single out and Pierotti[9] has shown that treating data obtained using a

heterogeneous adsorbent with a potential assuming a uniform surface results in an area which is smaller than that which would be obtained by assuming a potential function which reflected the surface heterogeneity.

The Significant Structures Theory

The virial theory allows a relatively exact treatment of physical adsorption phenomena, but its usefulness for interpreting data is normally restricted to coverages on the order of a tenth of a monolayer or less. The important range between a tenth and one monolayer is treated using intuitive and less exact statistical thermodynamic models. With these models it becomes possible to treat phase transitions and critical phenomena.

The significant structures theory of the liquid state[33] has been modified and applied to physical adsorption data by Pierotti and McAlpin[34] as well as others with considerable success. Newsome[2] has recently extended the theory to include multilayer formation.

The significant structures model of submonolayer physical adsorption is developed according to the following scheme after Pierotti and Thomas.[9] The adsorbate is divided into an adsorbed phase and a vapor phase. The vapor phase is considered ideal, consequently its partition function is known. The potential energy of the adsorbed phase is divided into a component in the plane of the surface (x,y) and a component perpendicular to the surface (z). The z component is treated as a harmonic oscillator thus its potential function and partition function are known. The complex (x,y) component which contains all of the distribution and lateral interaction dependence is treated as a two-dimensional significant structures fluid resulting in a partition function which, when

combined with the z component, gives the partition function for the adsorbed phase. Functions for the chemical potential of the adsorbate in both phases are derived from these partition functions, and then equated resulting in the desired isotherm equation.

The adsorbed atoms are "bound" to the surface in the sense that they are constrained to execute small vibrations about their equilibrium distance above the surface (z^*) but are free to translate in the plane of the surface. The volume of the adsorbed phase then is Az^* where A is the area of the adsorbent, and that of the vapor phase is $V - Az^*$ where V is the volume available to the adsorbate.

If all of the interactions in the system are taken as pairwise additive, the total potential energy of the adsorbate may be written

$$U_T = \sum_i U_{g,S}(\bar{r}_i) + \sum_{\text{All Pairs}} U_{g,g}(\bar{r}_i, \bar{r}_j) \qquad (20)$$

where

$U_{g,S}(\bar{r}_i)$ is the potential arising from gas-solid interactions

$U_{g,g}(\bar{r}_i, \bar{r}_j)$ is the potential arising from interactions between pairs of adsorbate atoms.

If the total potential is separated into a component in the plane of the surface and another perpendicular to the surface, the result may be written

$$U_T = \sum_i U_{g,S}(z_i) + \sum_i U_{g,S}(\bar{\tau}_i) + \sum_{\text{All Pairs}} U_{g,g}(\bar{\tau}_i, \bar{\tau}_j) \; . \tag{21}$$

where $\bar{\tau}$ is a vector which gives the position of an adsorbate atom in the plane of the surface. This separation is only possible when the adsorbed film is planer or its density is very low.

The vibrations have been taken as being small, consequently, it is reasonable to treat the z dependent component with a one-dimensional harmonic oscillator potential. In the case of krypton the oscillator may be considered classical. This component of the potential is then given by

$$U_{g,S}(z_i) = - \epsilon^*_{1,S} + \tfrac{1}{2} k_z (z_i - z^*_i)^2 \tag{22}$$

where

$-\epsilon^*_{1,S}$ is the minimum in U(z) and

k_z is the force constant for the gas-solid interaction.

The canonical partition function for a gas in a volume V and at a temperature T which is interacting with a surface may be written

$$Q_N = Z_N(V,T)/\Lambda^{3N} N! \tag{23}$$

where $Z_N(V,T)$ = the N particle configuration integral for the system

$\Lambda = (h^2/2\pi mkT)^{\frac{1}{2}}$

h = Planck constant

m = atomic mass

N = number of adsorbate atoms present.

When the potential energy is separated as indicated above, Q_N may be factored according to

$$Q_N(V,T) = \frac{Z_N(\bar{\tau},T)}{\Lambda^{2N} N!} \cdot \frac{Z_N(z,T)}{\Lambda^N} \quad . \tag{24}$$

With the harmonic oscillator assumption, $Z_N(z,T)$ may be reduced to give

$$\frac{Z_N(z,T)}{\Lambda^N} = \left[\frac{kT}{h\upsilon_z}\right]^N \exp\left\{\frac{N\epsilon^*_{1,S}}{kT}\right\} \tag{25}$$

where υ_z is the classical frequency of the oscillator. The treatment of $Z_N(\bar{\tau},T)$ is more complex and it is here that the significant structures theory is utilized.

The significant structures theory may be rationalized as follows. The constituent atoms of an atomic solid are constrained to vibrate about their position in a virtually complete lattice. When melting occurs the density of the liquid is generally found to be lower than that of the

solid, but diffraction studies indicate the nearest neighbor distance in the liquid is almost identical to that observed in the solid. According to the significant structures theory this decrease in density or increase in molar volume upon melting is due to the introduction of vacancies into the lattice of the solid. These vacancies or more precisely the ability of neighboring atoms to move into a vacancy results in the increased mobility characteristic of the liquid state.

In a two-dimensional significant structures fluid, an atom may find itself in one of three environments: it may be surrounded by nearest neighbors and thus constrained to vibrate about its equilibrium position as in the solid, a nearest neighbor may be missing producing an asymmetric field about the atom and resulting in what might be called a strained solid, or a significant fraction of neighboring positions might be vacant thus allowing the atom to translate as though it was in a gas. The significant structures partition function for the two-dimensional phase is derived from an appropriately weighted statistical averaging of these three states or structures. It can be shown[9] that this partition function is given by

$$Q_N(A_a,T) = q_{2,s}^{\theta^2 N_m} \, q_{2,g}^{\theta N_m (1-\theta)} \tag{26}$$

where

A_a = area of the adsorbed phase

$q_{2,s}$ = molecular partition function for a configurationally degenerate two-dimensional solid

$q_{2,g}$ = molecular partition function for a two-dimensional gas

θ = ratio of number of atoms adsorbed to number adsorbed at monolayer coverage

N_m = number of atoms adsorbed at monolayer coverage.

Finally models and consequently the partition functions for the two-dimensional gas and degenerate solid must be chosen. The gas-like state will be considered an ideal two-dimensional gas, consequently

$$q_{2,g} = \frac{\Lambda^{-2} e a_m^o}{\theta} \tag{27}$$

where

e = the base of the natural logarithms

a_m^o = area per molecule at monolayer coverage.

The solid-like state will be treated as a degenerate cell or Lennard-Jones and Devonshire[35] solid thus

$$q_{2,s} = \Lambda^{-2} a_f e^{W/kt} [1 + c(1 - \theta)/\theta] \tag{28}$$

where

$a_f \equiv$ free area

$$= \pi a^2 \int_0^{a/2} \exp \left\{ \left(\frac{c\epsilon^*_{1,2}}{kT} \right) x \left[1_S(y) - 2m_S(y) \right] \right\} dy \qquad (29)$$

a = average distance between nearest neighbor atoms in adsorbed film

c = coordination number of the lattice of the adsorbed film when there are no vacancies

$1_S(y), m_S(y)$ are polynomials given by Lennard-Jones and Devonshire

$\epsilon^*_{1,2}$ = minimum in the potential between two atoms interacting in the adsorbed phase

W = the lattice energy of a two-dimensional solid of N atoms.

Substituting equations (27) and (28) into equation (26) the total partition function for the two-dimensional significant structures fluid is found to be

$$Q_N(A_a,T) = \Lambda^{-2\theta N_m} \left[a_f \exp \left\{ \frac{W}{NkT} \right\} \left(1 + \frac{c(1-\theta)}{\theta} \right) \right]^{\theta^2 N_m} \left[\frac{a_m^o e}{\theta} \right]^{\theta N_m (1-\theta)} \qquad (30)$$

Noting that $Q_N(A_a,T) = \dfrac{Z_N(\bar{\tau},T)}{\Lambda^{2N} N!}$ and recalling equations (24) and (25), it is found that $Q_N(V,T)$, the canonical partition function of the adsorbed film, is given by

$$Q_N(V,T) = \left[\Lambda^{-2}\left(\frac{kT}{h\nu_z}\right) \exp\left\{\frac{\epsilon^*_{1,S}}{kT}\right\} \right]^{\theta N_m}$$

$$\times \left[a_f \exp\left\{\frac{W}{NkT}\right\}\left(1 + \frac{c(1-\theta)}{\theta}\right) \right]^{\theta^2 N_m} \qquad (31)$$

$$\times \left(\frac{a^o_m e}{\theta}\right)^{\theta N_m(1-\theta)} .$$

The chemical potentials of the adsorbate in both phases can now be derived and when these are equated the desired isotherm equation is found to be

$$f = K_{S,S}\left[\left(\frac{e a^o_m}{a_f}\right) \exp\left\{-\frac{W}{kT}\right\}\right]^{2\theta} \exp\{-g(\theta)\} \qquad (32)$$

where

$K_{S,S}$ ≡ the significant structures Henry's law constant

$$= \frac{h\nu_z}{\Lambda e a^o_m} \exp\left\{-\frac{\epsilon^*_{1,S}}{kT}\right\}$$

$$g(\theta) = 2\theta \ln\{\theta[1 + c(1 - \theta)/\theta]\}$$

$$- \ln\theta - \frac{(c - 1)\theta^2}{c - (c - 1)\theta} - 1.$$

The BET Theory

The theory of Brunauer, Emmett, and Teller,[8] called the BET theory after the authors, is based on the Langmuir isotherm equation, the oldest of such equations. The physical model which it represents is less realistic than that of most theories which have followed, but it is mentioned here because of its practical and historical significance and because it represents a different view of the adsorbed phase. Also the theory was used to obtain the surface areas of the copper crystals and the sample cell involved in these experiments.

Hill[36] has shown that the Langmuir equation results if the adsorbed phase is considered an ideal two-dimensional lattice gas. The gas-solid potential is assumed to provide an array of M equivalent, distinguishable, and independent sites or small areas into which only one of the N_a adsorbed atoms may be placed. An atom can be adsorbed and desorbed from a site but it cannot translate across the surface from site to site. The Langmuir model then is an example of a localized model of adsorption, i.e., no translation in the (x,y) plane, whereas the two previous models were examples of mobile models. Finally, no lateral interactions are allowed and the surface coverage may not exceed a monolayer, i.e., $N_a \leq M$.

If all of the sites are filled, the canonical partition function for the adsorbed phase is given by

$$Q(N_a,T) = q(T)^{N_a} \tag{33}$$

where

$q(T)$ = the molecular partition function for an adsorbed atom.

In the case of interest where some of the sites are unoccupied the lattice gas is configurationally degenerate and the partition function becomes

$$Q(N_a,M,T) = \frac{M!\,q(T)^{N_a}}{N_a!\,(M-N_a)!} \tag{34}$$

where $\frac{M!}{N_a!\,(M-N_a)!}$ is the number of ways N_a indistinguishable atoms may be distributed over M labeled sites.

If the harmonic oscillator approximation is now used for $q(T)$ and the adsorbate vapor is assumed ideal, the Langmuir equation is obtained

$$\theta(P,T) = \frac{\chi(T)P}{1 + \chi(T)P} \tag{35}$$

where

$$\chi = q(T)e^{\mu^{\circ}(T)/kT}$$

μ° = standard state chemical potential of the adsorbate vapor.

Equation (35) then allows the calculation of the adsorption isotherm from atomic properties.

A more common form of the Langmuir equation is given by

$$V_a = \frac{V_m bP}{1 + bP} \tag{36}$$

where

V_a = the STP volume of gas adsorbed

V_m = volume of gas adsorbed at monolayer coverage thus $\theta = \frac{V_a}{V_m}$ and

$$b = \chi(T).$$

The BET theory is an extension of the Langmuir theory to take into account multilayer formation, i.e., $N_a > M$. The additional assumptions made are that the multilayers must be formed by atoms residing above a previously adsorbed atom, i.e., columns of adsorbed atoms are formed above each site, and that the energy change upon adsorption is the same for an adsorbate atom in any layer above the first. With these assumptions the isotherm equation is found to be

$$\frac{V_a}{V_m} = \frac{CX}{(1 - X + CX)(1 - X)} \tag{37}$$

where

$$C = q_1/q_2$$

$$X = q_2 e^{\mu^o/kT} P = \frac{P}{P_o}$$

q_2 = the atomic partition functions for all of the adsorbed atoms above the first layer

P_o = the saturation vapor pressure of the adsorbate at the temperature of the isotherm.

The BET theory has been widely applied to the determination of surface areas. For this purpose it is usually rearranged into the following form:

$$\frac{X}{V_a(1 - X)} = \frac{1}{V_m C} + \frac{(C - 1)X}{V_m C} \quad . \tag{38}$$

If the left hand side of equation (38) is plotted against X and C is constant over the range of the data used, the slope and intercept of the resulting curve allow the calculation of V_m and C. If an area is then assigned to each site, the area of the adsorbent may be calculated from V_m. Because of the unrealistic nature of the BET theory, the molecular parameters which result from using it to interpret experimental data are of little value. It has, however, provided a method for systematically determining the surface area of adsorbents.[8]

Statement of the Problem

The goal of the work presented here was to obtain information about the forces acting at the gas-solid interface.

The copper-krypton system was chosen for the following reasons:

(a) An understanding of the forces at the gas-metal interface is of considerable importance and little useful data are available.

(b) Sinanoğlu and Pitzer have predicted that the effect of a metallic surface on the forces between adsorbed atoms should be relatively great, consequently, this effect should be more easily detected on a metallic surface.

(c) Seed crystals were available for growing copper crystals with

other lattice indices in the plane of the surface, thus making it possible to determine the importance of the effect of the orientation of the metallic cores on the interfacial forces in future studies.

(d) The copper-krypton system was expected to provide data over a wide range of coverages (θ) within the temperature range attainable with the adsorption apparatus.

The method of attack on the problem was to:

(a) Construct an ultra-high vacuum adsorption apparatus and cryostat which would provide meaningful data with the small area of copper surface available.

(b) Obtain copper-krypton isotherms over the range of temperatures accessible with the cryostat.

(c) Determine the interaction parameters ($\epsilon^*_{1,S}$, $\epsilon^*_{1,2}$) for the system by applying the virial and significant structures theories to the data.

(d) Indicate what new information the interaction parameters provided about the gas-metal interface.

CHAPTER II

ADSORPTION APPARATUS

Three characteristics of the copper crystals to be investigated were of primary importance in developing the design of the adsorption apparatus.

(1) Small surface area of the sample: Volumetric adsorption experiments normally involve samples with sufficiently large surface areas, relative to the volume of the sample cell, to insure that most of the adsorbate is in the adsorbed state rather than in the vapor phase. This reduces the importance of errors in the measurements of the equilibrium pressures (P_e) and in the volume calibrations. The copper crystals, however, had a very small surface area (approximately 80 cm^2), consequently, the volume of the sample cell had to be minimized and the equilibrium pressure measurements had to be made with a high degree of accuracy. In addition, the walls of the sample cell had an area of about 50 cm^2. This meant that each isotherm point had to be corrected for background adsorption, thus approximately doubling the accuracy required of the apparatus in order to maintain a given level of accuracy in the isotherm results.

(2) Chemical reactivity of copper: The adsorption system had to be free of mercury to prevent contamination of the copper crystals. This requirement and the high order of accuracy needed in the pressure measurements led to the choice of a capacitance manometer as the pressure measuring device. Provision was also made for hydrogen

reduction of the copper sample to assure that its surface was free of oxide.

(3) Surface contamination: The copper surface shows a great affinity for a number of materials commonly observed as residual gases in vacuum systems. Consequently, an ultra-high vacuum adsorption apparatus was required to maintain sufficiently low levels of these contaminants to provide an atomically clean surface for study.

The instrument constructed for this study consisted of two principal parts: an ultra-high vacuum volumetric adsorption apparatus and a cryostat. Both of these systems will now be discussed in detail.

Volumetric Adsorption Apparatus

Ultra-High Vacuum System

The ultra-high vacuum section of the apparatus was bounded by valves 2, 3, and 6 (Figure 3). All of the components in this section were compatible with an ultra-high vacuum environment. The connecting tubing was kovar, glass, and stainless steel. With the exception of the sample cell flange, the demountable seals used were Granville-Phillips "Conflat" flanges or Cajon "VCR" couplings. All of the permanent metal to metal seals were arc welded in an inert atmosphere or brazed with a gold-nickel alloy in a hydrogen atmosphere. Metal or glass bellows were placed in critical locations to relieve the stresses created during heat cycling. The valves in this section were obtained from Granville-Phillips and fell into three categories: Valves 5, 6, 7, and 8 were series 203 variable leak valves, valves

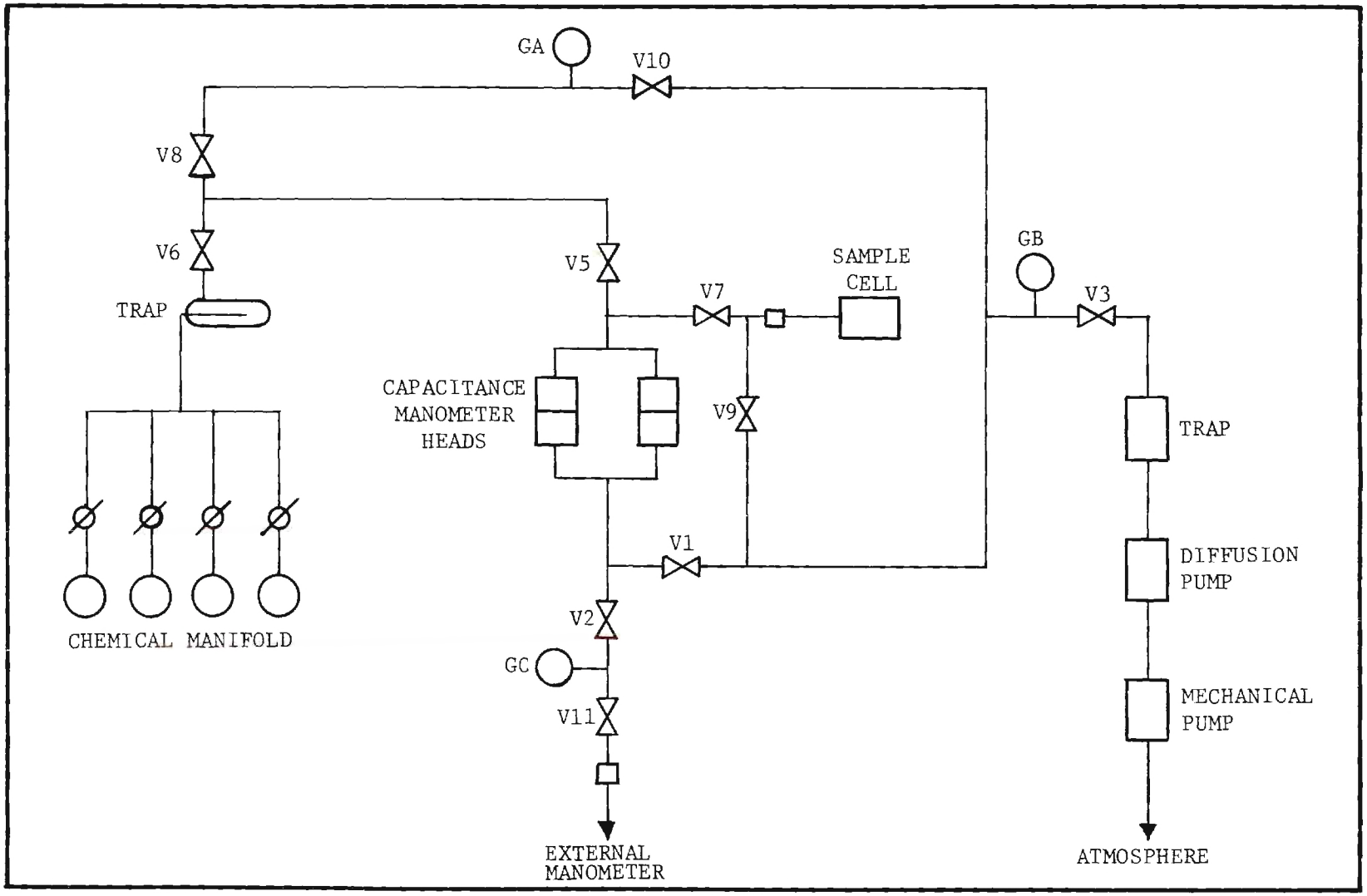

Figure 3. Schema of Adsorption Apparatus

1, 2, 9, and 10 were series 202 (Type C) "on-off" valves and valve 3 was a series 204 (Type L) 1 in. "gate" valve. Gauges A and B were Veeco RG75P ionization gauges.

Pumping System

The pumping system was purchased as a unit from Granville-Phillips (series 225 pumping station). It consisted of a 2 in. three stage fractionating diffusion pump charged with Dow Corning fluid 705, a Welch Duo-Seal forepump, and a baffled "Cryosorb" trap.

In addition to producing the very low pressures required for the experiment, the pumping system had to prevent the backstreaming of diffusion pump oil which might contaminate the sample. The combination of the very low vapor pressure of fluid 705 and the superior design of the "Cryosorb" trap seemed to meet these requirements.

Chemical Maniford

The chemical manifold was designed to provide the various gases required during the experiment. The gases stored here were: two 1/2 l. pyrex bottles of krypton, one 1 l. pyrex bottle of hydrogen and one 1 l. bottle of helium. These gases were obtained from Air Products and Chemicals as analyzed reagent grade and accompanied by batch analyses.

The stopcocks used in the manifold were Eck and Krebs 2 mm. cupped stopcocks. Apiazon L grease was used in order to minimize the introduction of stopcock grease into the manifold. A small trap was included just prior to valve 6 to capture any low vapor pressure material which found its way into the manifold.

External Manometer Port

The vacuum system on the outside of valve 2 allowed indirect

pressure measurements with a mercury manometer. A Veeco thermocouple gauge (C) and a Nupro "4 BK" valve (11) were used here. Connection to the external manometer system was made through a 1/4 in. Swaglok *fitting machined* on the Nupro valve body.

This port was also used as an inlet for interfacing with a helium mass spectrometer leak detector (Veeco model MS9AB)。 The mass spectrometer allowed the locating of very small real leaks in the vacuum system; a capability which is very important in this type of experiment.

Sample Cell Assembly

The sample cell assembly consisted of three parts: an ultra-high vacuum fitting which connected the assembly to the adsorption apparatus, a length of 1/8 in。 O.D. metal tubing, and the cell itself. A Cajon "4 VCR" ultra-high vacuum coupling was used to attach the sample cell line to the adsorption system. This coupling was bored out along its long axis and copper tubing was slid through from the back to the face of the coupling until a short neck of tubing protruded past the face. A coil of gold-nickel brazing alloy was slipped over the neck and the seal was formed in a furnace filled with hydrogen. The excess tubing and brazing alloy were machined away leaving a flush seal at the face of the coupling. Initially, a length of 1/8 in. O.D. copper tubing ran from the coupling to the sample cell, but it was found that after repeated baking cycles, the copper tubing just above the sample cell developed hairline cracks。 Copper had been chosen as the material to be used in this part of the system because of its chemical stability under the conditions of the experiment but

it had to be abandoned and an equally well suited substitute could not be found. The only alternative available proved to be type 304 stainless steel tubing which was known to form a thin oxide film under the conditions used to reduce the copper sample. The oxidation problem was overcome by oxidizing the tubing prior to beginning the isotherm determinations. The effect of using stainless tubing was to increase the roughness factor of the cold portion of the sample cell assembly. The stainless tubing extended from the sample cell, out the top of the cryostat where it was brazed to the copper tubing coming from the adsorption apparatus.

The sample cell had been machined from nickel for an earlier study[37] (see Figure 4). The design of the seal was that of Steckelmacher[38]. A thin neck was machined into the face of the sample cell top so that the stainless steel tubing could be welded to the inside face. The weld was made with an arc under an argon atmosphere. The sample cell top was polished to a mirror finish by first burnishing with steel wool and then rubbing the face on a flat surface covered with a very fine abrasive dust in a lubricating fluid.

Before inserting the copper sample, the inside of the sample cell was electropolished using a 25 percent perchloric acid, 75 percent acetic acid electrolyte. A piece of 1/4 in. O.D. stainless steel tubing was suspended along the axis of the cell cavity and used as the cathode. A very bright surface was obtained.

A copper gasket was used to effect the seal between the top and body of the sample cell. The gasket was formed and then annealed at approximately 700°C in a vacuum furnace. The sealing

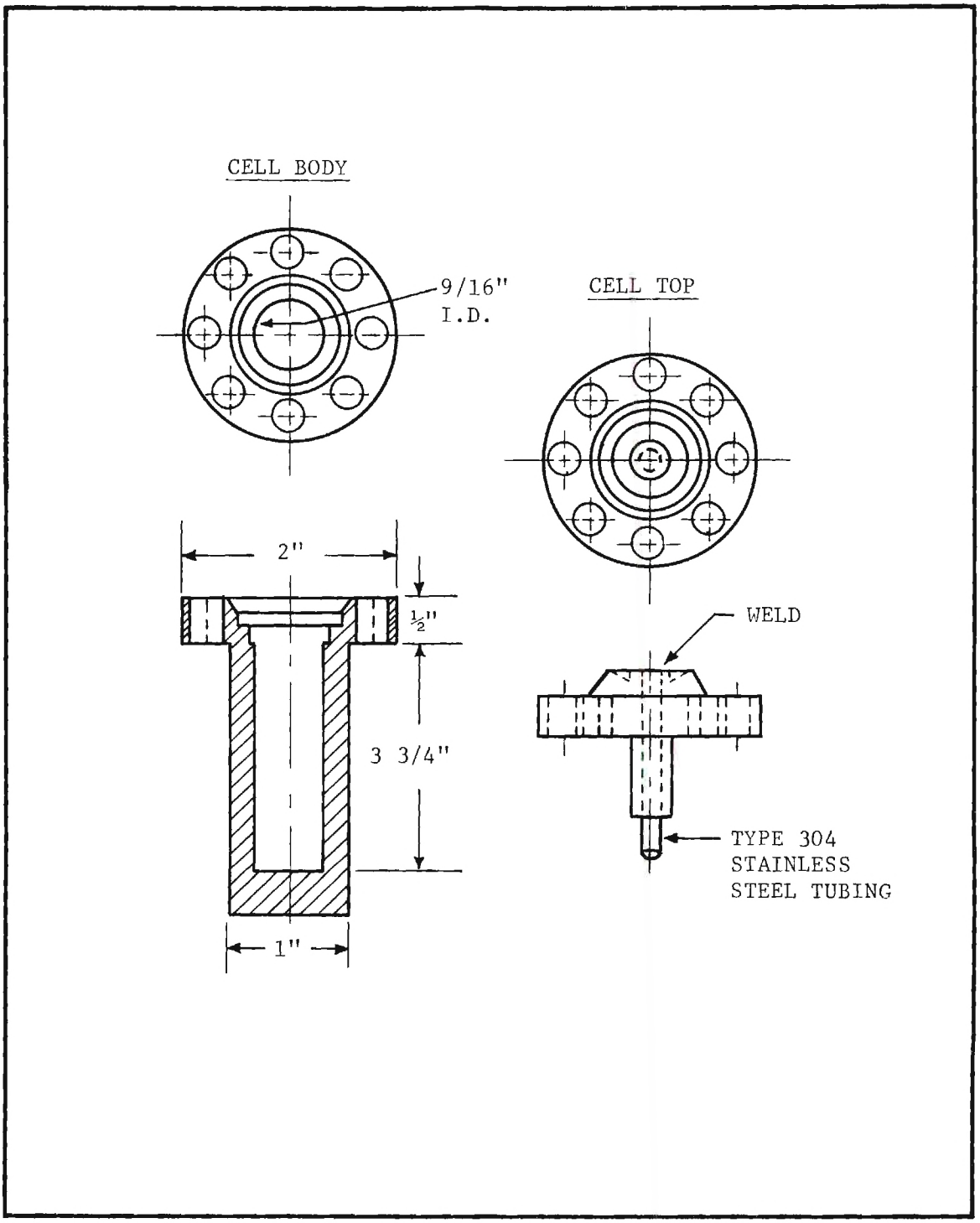

Figure 4. Sample Cell Assembly

surfaces were brought together by eight stainless steel bolts. The seal never failed even under the extreme thermal cyling of the experiment.

Capacitance Manometers

Two MKS "Baratron" (MKS Instruments, Inc., Burlington, Mass.) capacitance manometer heads were used to make the high precision pressure measurements required. These heads were designated 90H-1 and 90H-300 by the manufacturer. The 90H-1 head had a range of from 0.0003 to 1 torr full scale and the 90H-300 head ranged from 0.1 to 300 torr. These two heads were used in conjunction with the manufacturer's 90M-XRP-2 dual channel indicator, and a 1090-2 head temperature control unit was installed to provide maximum stability.

The 90H series of manometer heads was specifically designed for use in an ultra-high vacuum environment. The diaphragms were made of inconel "X" and the other surfaces which were exposed to the vacuum system were nickel, type 304 stainless steel, and ceramed glass. The heads were of all welded construction and no organic materials were present. The manufacturer claimed that these heads could be baked to 350^{o}C with very little change in calibration.

The capacitance manometer output was recorded on a Hewlett Packard strip chart recorder (Model 680).

Bake Out Oven and Air Thermostat

An oven was constructed around the ultra-high vacuum portion of the system. This oven was to serve the dual prupose of providing for high temperature baking of the apparatus and also for thermostating of the apparatus during adsorption measurements.

The oven was constructed of 1 in. thick "Marionite" (Johns-Manville) medium density asbestos board. The oven top was counter weighted for easy access and the front and left side of the oven could be removed. Four flat heating units were attached to the oven top with "Transite" (Johns-Manville) supports. These units were obtained from Fisher Scientific and were rated at 1 KVA each. Two of the heating units were wired to operate at line voltage and were used only during a bakeout. Each of the other two units were powered by a 9 amp. variable voltage supply. These two heaters were operated by a YSI temperature controller which regulated the oven temperature during an isotherm determination. Thermal gradients in the oven were reduced by stirring the air bath with two 5 in. "Wisper Fans" by Rotron. These wafer fans were found to provide excellent stirring while introducing little heat or vibration into the oven.

Temperature Measuring System

Temperature measurements were made with thermocouples positioned at critical points around the adsorption system. The thermcouple EMF's were measured in the usual way with a water-ice reference bath. The elements of the circuit were as follows:

Thermocouples -- Copper-constantan made from Leeds and Northrup 24 gauge thermocouple wire

Potentiometer -- Leeds and Northrup model K-2

Galvanometer -- Leeds and Northrup Type E

Thermocouple selector switch -- Leeds and Northrup model 8248-10 10 position rotary switch

Standard cell -- Eppley Laboratories saturated reference cell

Working voltage source -- Leeds and Northrup 099034 3V constant voltage supply.

All of the thermocouple beads were formed by carefully melting the twisted wire under silver solder flux. With care this technique produced a bead which appeared comparable to those formed with a DC arc in a reducing atmosphere. The three thermocouples which were placed in the cryostat were covered with a thin layer of epoxy resin to prevent mechanical or chemical changes in the thermocouples which might lead to calibration changes.

Main Power Supply

All of the instruments and the oven heaters were operated by power from two 9 amp. Solar regulated power supplies. The apparatus had a current regulating system which prevented overloading the power supplies.

Mercury Manometer

Figure 5 shows the mercury manometer system used in various calibration procedures. The two traps in the system were long and narrow to prevent the diffusion of mercury from the manometer tubes into the adsorption apparatus. The Fisher-Porter valve on the vacuum line allowed very precise balancing of the pressure across the capacitance manometer. The measuring portions of the mercury manometer arms were made of 2 cm. O.D. thin wall tubing to minimize capillary depression and the connecting U-tube was made of 1 mm. capillary tubing.

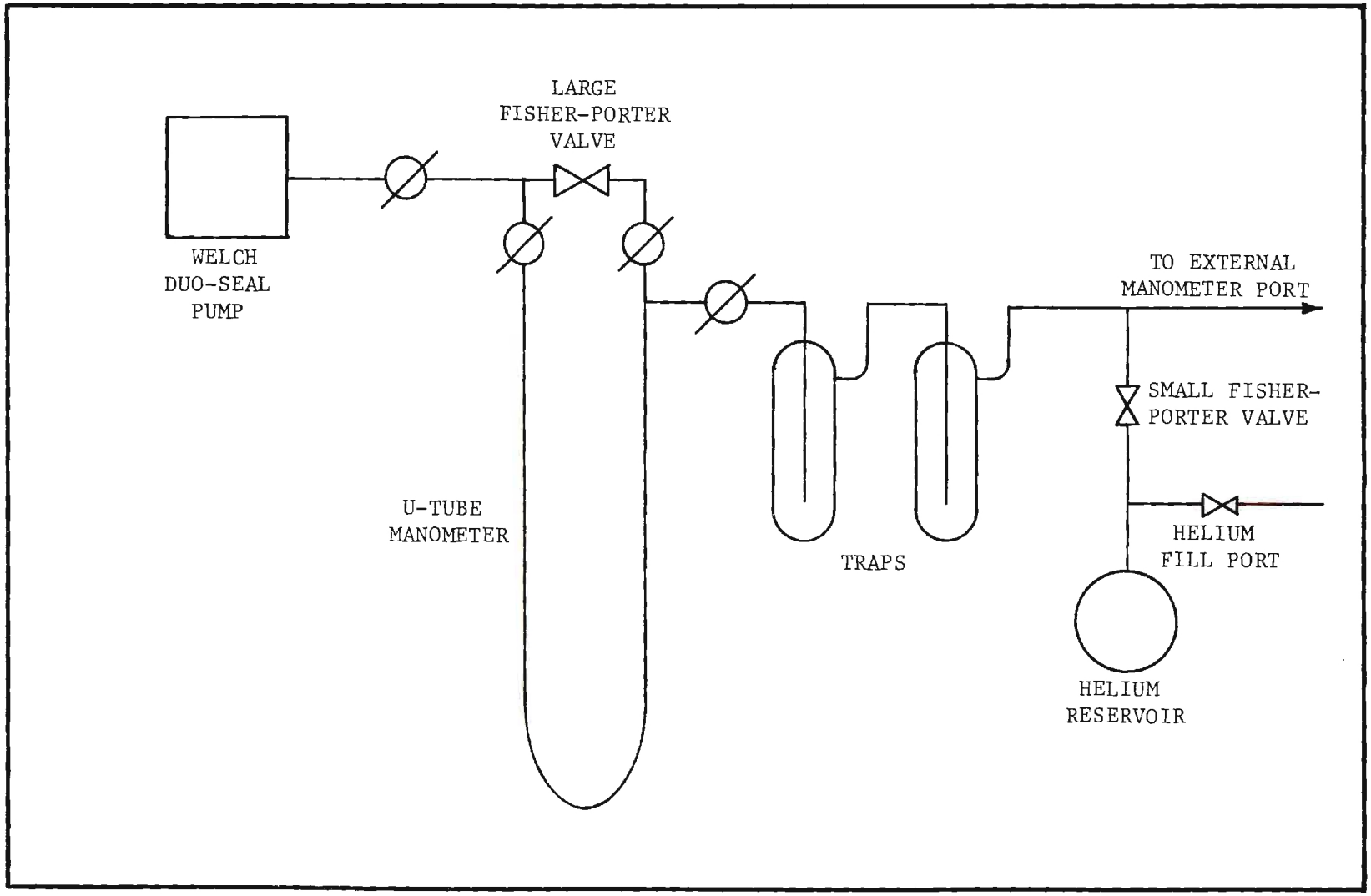

Figure 5. External Mercury Manometer System

Cryostat

A high pressure cryostat was constructed for this study which used liquid nitrogen as the cryogenic bath and could achieve any temperature in the range of from 78° to 108°K. A schema of the system is shown in Figure 6.

Simply stated, the mode of operation of the cryostat was to control the bath temperature by controlling the pressure of the vapor in equilibrium with the bath fluid. A cryostat of this type has been described[39] except that the bath temperature was controlled by holding the vapor pressure constant. The cryostat described here overcomes certain difficulties inherent in this approach by using the bath temperature directly as the controlling parameter. This was achieved by utilizing a vapor pressure thermometer immersed in the bath as the controlling element.

The cryostat consisted of a high pressure thermally insulated container, a system for regulating the bath temperature, and a system to maintain a constant liquid nitrogen level in the bath. Each of these components will now be described in detail.

High Pressure Container (Figure 7)

A container for the cryostatic bath was required which allowed minimum heat influx while safely withstanding internal pressures of up to 200 psig. Commercial dewars which met these requirements were investigated and it was found that such dewars, though quite expensive, allowed a substantial heat influx. The following design was then developed which met the requirements of the system at a nominal cost.

A 15 in. long section of 6 in. I.D. schedule 40 carbon steel

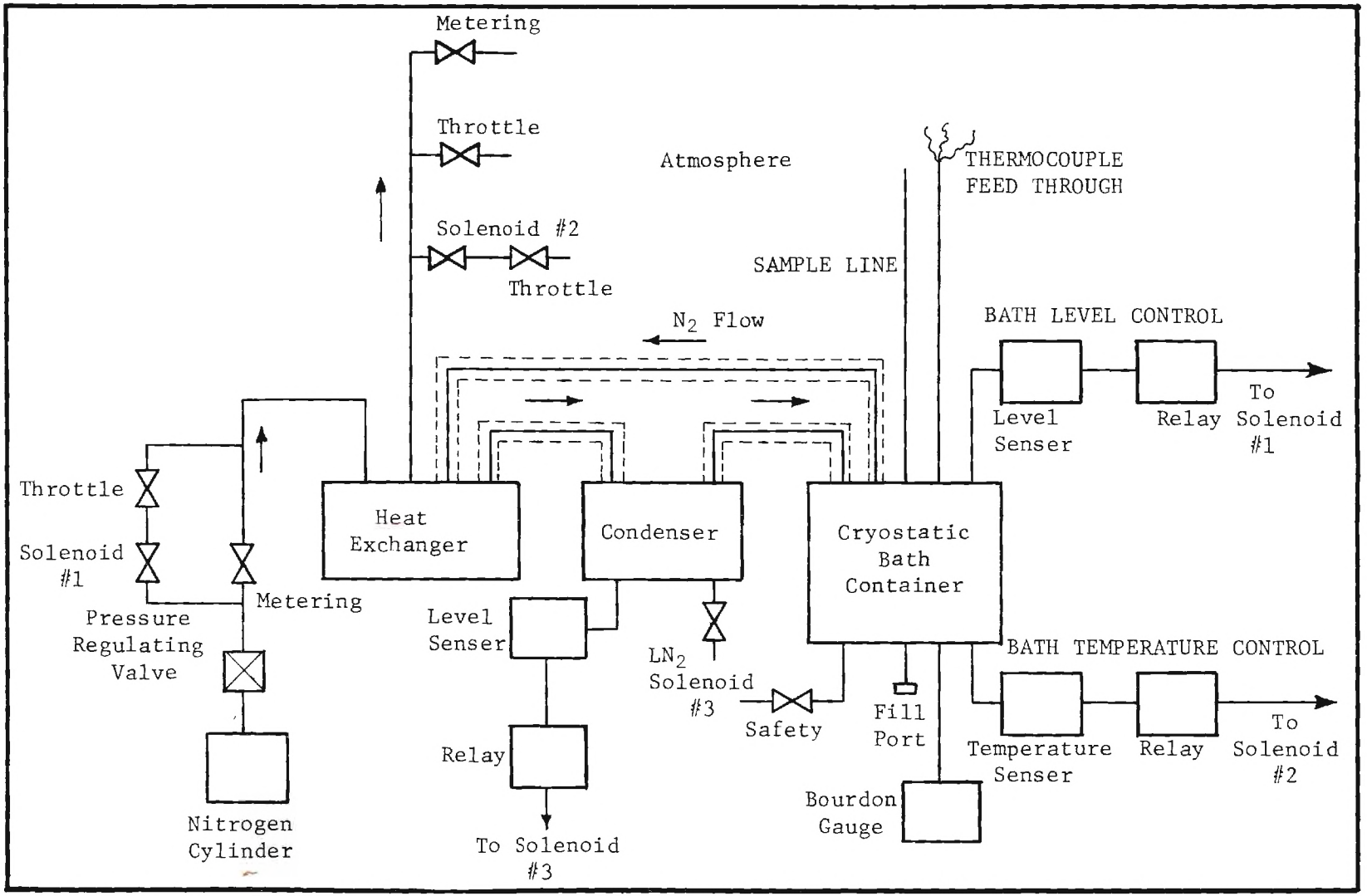

Figure 6. Schema of Cryostat

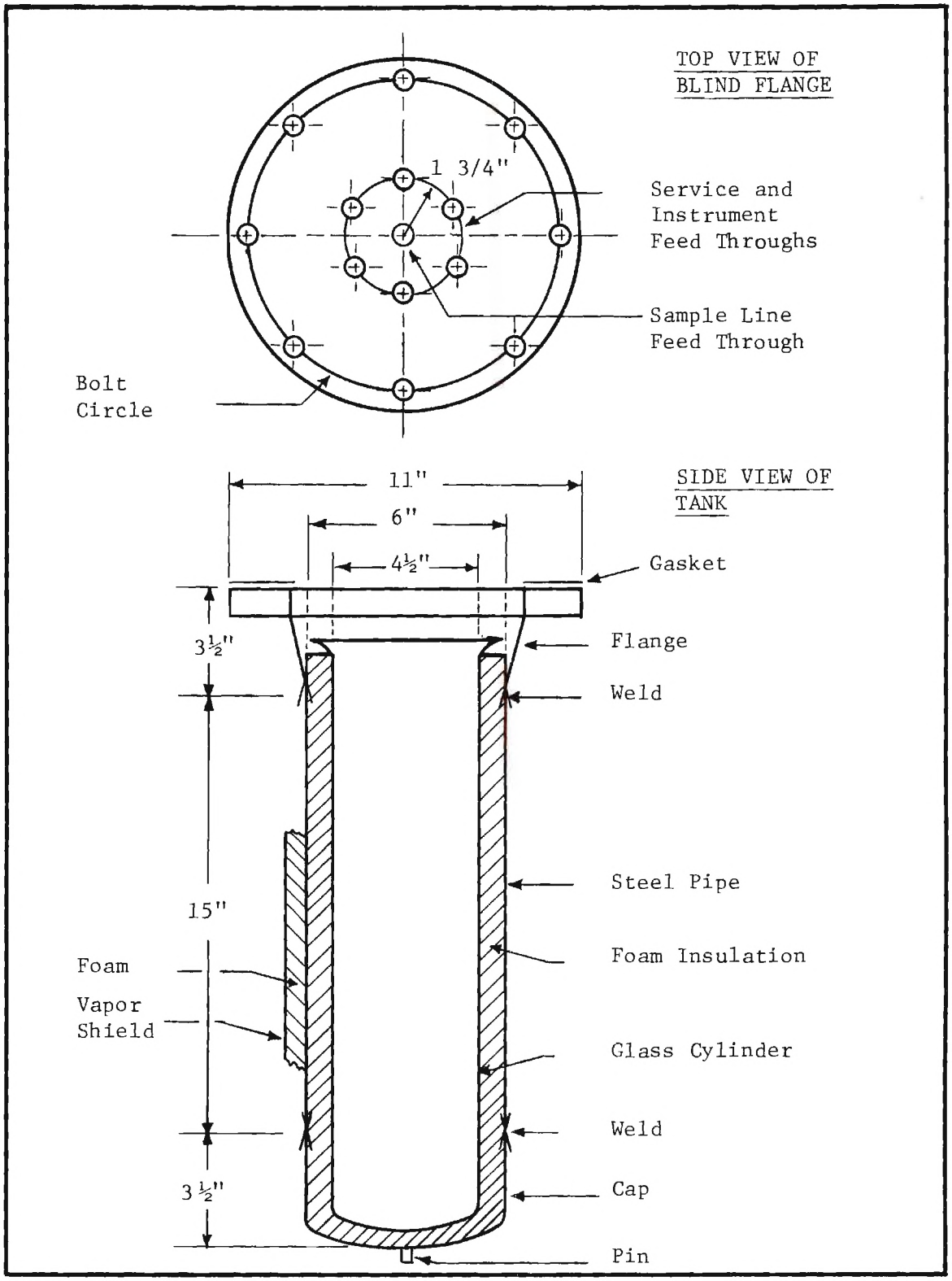

Figure 7. High Pressure Container for Cryostatic Bath

pipe was welded to a "standard" Grinnell cap on one end and a 150 pound Grinnell welding neck flange on the other. The pipe was properly beveled and welding rings with spacers were used to insure complete weld penetration. The tank thus constructed was cleaned and painted.

A sheet of 1 in. thick medium density foam rubber was contoured to cover the inner wall of the tank and a 4 1/2 in. O.D. by 19 in. long glass tube with a closed and rounded bottom and a flared top was slid into the foam jacket. The glass cylinder had a volume of approximately 5 liters and was to be the container for the boiling liquid nitrogen bath.

A 6 in. "150 lb." Grinnell blind flange completed the cryostat vessel. This flange was drilled and tapped to allow access for the numerous controls and plumbing required in the operation of the cryostat. Two brackets were welded on opposite sides of the blind flange and it was permanently attached to the frame which housed the cryostat. To allow access to the sample cell which resided in the cryostat, the tank was attached in such a way as to allow it to be raised or lowered from the blind flange. Alignment of the tank and flange was assured by two aluminum rods which ran through guides welded to the sides of the tank. Raising and lowering the heavy vessel was accomplished by a two ton capacity scissor jack from Sears Roebuck and Company. A pin welded to the bottom of the tank prevented it from slipping off the jack.

The cryostat vessel was sealed by raising the tank to the blind flange and bolting the flanges together with a rubber impregnated asbestos gasket in between. Eight 5/8 in. diameter bolts were used to

secure the seal. When the cryostat was sealed and ready for operation, additional insulation was placed around the tank. This insulation consisted of contoured 1 in. thick medium density foam rubber which was covered with a plastic bag to reduce the rate of condensation of atmospheric moisture in the insulation.

Bath Temperature Control

The temperature was held constant by a vapor pressure thermometer immersed in the bath. This thermometer formed the sensing element of a control circuit which regulated the rate of escape of N_2 vapor from the cryostat tank, thus adjusting the pressure above the bath and maintaining the temperature within close limits.

The fluid used in the vapor pressure thermometer depended on the temperature desired. Argon was used from 78°K up to its normal boiling point at 86°K and krypton was used above 86°K.

The probe of the vapor pressure thermometer consisted of a length of 1/4 in. O.D. copper tubing which entered the cryostat through a bored out Swaglok fitting and extended to just below the bottom of the sample cell. This end of the probe was crimped and sealed with silver solder. The upper end of the probe went to a manostat and a gas manifold. The manostat, consisting of a U-tube mercury manometer with equally spaced electrical contacts on its reference side, converted the vapor pressure changes in the probe to the electrical signal required by the control circuit.

The vapor pressure thermometer probe could be filled with either krypton or argon from the manifold which also provided a vacuum source (Welch Duo Seal pump) and atmospheric bleed allowing

fine control over the pressure on the reference side of the manostat. This control was used to establish the temperature desired in the cryostat.

The manostat was the control element for a Sargent Laboratory Relay which in turn operated an ASCO (827616R) solenoid valve in series with a Whitey (31RS4) throttle valve. N_2 gas was allowed to constantly escape from the cryostat through two metering valves (Whitey 3RS4 and 22RS4). These valves were adjusted, however, so that the pressure above the bath would slowly rise causing the bath temperature to rise. When the vapor pressure thermometer sensed an increase in bath temperature, the solenoid valve opened and additional gas was allowed to escape. The rate of gas loss through the solenoid was adjusted so that the pressure above the bath would fall below that of the temperature desired. When this occurred the solenoid closed, thus starting the cycle over. The gas emission system was tuned during a run so that the duration of the solenoid open cycle was approximately equal to its closed cycle.

Bath Level Control

Controlling the vapor pressure above a boiling liquid nitrogen bath is a relatively easy means of obtaining temperatures in the difficult range just above the boiling point of liquid oxygen. The principal difficulty is replacing the nitrogen which evaporates from the bath. Maintaining the bath level by filling directly from a storage dewar is impossible because such dewars are not engineered to withstand pressures in excess of two atmospheres. A simple solution and the one used here is to condense nitrogen gas at a pressure

above that in the cryostat and subsequently blow the concensate into the cryostat bath.

The bath level monitoring device consisted of a probe connected to a simple two contact manostat. The probe was a length of 1/4 in. O.D. copper tubing which entered the cryostat through a bored out Swaglok fitting in the blind flange. The extension of the probe was adjusted so that its crimped and soldered tip was at the position desired for the top of the liquid nitrogen bath, which was chosen as 2 in. above the top of the sample cell. With the probe and manostat in position the system was evacuated and filled with krypton. When the liquid nitrogen level rose to the tip of the probe, krypton sublimed thus dramatically reducing the pressure in the probe side of the manostat and bringing down the mercury column on the reference side. The manostat's electrical contacts were positioned so that at this point the circuit was open. When the liquid nitrogen level fell below the bottom of the probe, all of the krypton again entered the vapor phase and closed the contacts. The manostat controlled a Sargent Laboratory Relay which in turn activated the equipment required to return the liquid nitrogen level to the control point.

The nitrogen gas (prepurified grade from Air Products & Chemicals) destined to replenish the bath was obtained from a standard high pressure cylinder. The gas was first expanded through a 0-200 psig two-stage regulating valve, which adjusted the pressure of the gas so that it would be from 30-50 psig above that of the vapor in the cryostat. The gas then travelled through a parallel valve circuit. One arm of this circuit consisted of a fine metering valve (Whitey 22RS4) which allowed a slow constant flow of gas from the cylinder to the condensing system and the other arm consisted of a solenoid valve (ASCO 826820) in series with a

throttle valve (Whitey 31RS4). The solenoid valve was operated by the level monitoring device. When the liquid nitrogen level fell below the control point, the solenoid valve opened thus allowing a high flux of nitrogen gas into the filling system. The two arms of the circuit were tuned during a run so that the duration of the solenoid's open cycle was approximately equal to its closed cycle. The incoming gas then passed through a heat exchanger, which removed a significant amount of heat from the gas with a countercurrent flow of cold vapor escaping from the cryostat tank. The cooled gas then passed through an insulated line into the condenser, which consisted of a large helical coil formed from 1/4 in. copper tubing suspended in a dewar. The dewar was filled with liquid nitrogen boiling at atmospheric pressure, thus the nitrogen gas entering the coil condensed. When the bath level fell below the control point, the solenoid valve opened and the liquid nitrogen in the condensing coil was forced through an insulated line into the cryostat bath thus returning the level to the control point. A device similar to the level monitoring device in the cryostat was used to automatically fill the condenser dewar with liquid nitrogen from a vendor's pressurized dewar.

Miscellaneous Equipment

The tubing going to the sample cell entered the cryostat through a bored out 1/8 in. "Swaglok" fitting. A "Teflon" ferrule was used so that the position of the sample cell could be adjusted.

The cryostat was equipped with a 0-200 psig Bourdon gauge which was very useful for obtaining a rapid estimate of the bath temperature.

The weakest element in the pressure system was the blind flange which had a maximum operating pressure of 275 psig.[40] An Air Products

and Chemicals safety valve (17-4800) which automatically opened at 230 psig was installed in the pressure chamber to insure that the pressure could not exceed the safe working limits of the system.

A special feedthrough was attached to the blind flange which allowed three thermocouples to be placed in the bath. These thermocouples were used to monitor the sample cell temperature during an isotherm.

Finally, a 3/8 in. access port was provided so that the bath could initially be established by forcing liquid nitrogen from a storage dewar into the cryostat. During the initial filling the safety valve was removed to allow sufficient venting. When the bath level reached the control point, the port was sealed, the safety valve replaced, and the various systems previously described were set into motion.

Cryostat Operating Characteristics

The following operating characteristics were observed for the cryostat described here:

(1) Temperature range: 78° to 108°K using liquid nitrogen as the cryogenic fluid.

(2) Temperature reproducability: $\pm$ 0.2°K

(3) Temperature drift over operating period: < 0.02°K

(4) Temperature fluctuations about mean: < 0.05°K (twice the average standard deviation of the temperature data)

(5) Pressure range: slightly greater than 0 to 200 psig

(6) Rate of consumption of gaseous nitrogen in the bath filling process: 450 psig/hr* at 78°K

700 psig/hr* at 108°K

*From a standard cylinder.

(7) Rate of consumption of liquid nitrogen in the condensing system: approximately 9 liters/hr

(8) Duration of cryostat operation: 12 to 20 hours.

Calibration Procedures

Thermocouple Calibration

The three copper-constantan thermocouples which were used to determine the temperature of the sample during an isotherm measurement were calibrated against the vapor pressure of krypton. This allowed the calibration to span the entire temperature range of interest.

The procedure was as follows. The tubing leading into the sample cell was insulated in order to reduce the effect of any thermal gradients near the surface of the bath. The three thermocouples were taped together against the bottom of the sample cell. The adsorption system was pumped into the 10^{-8} torr range, the zero of the 300 mm capacitance manometer head was checked, and enough krypton was expanded into the sample cell to insure a two phase system for the vapor pressure measurements. The cryostat was filled with liquid nitrogen and allowed to vent freely to the atmosphere. The vapor pressure of the krypton in the sample cell was measured using the capacitance manometer. The EMF of each thermocouple was measured five times and the vapor pressure was determined after each reading. The cryostat was then sealed and set at three higher temperatures and the same set of measurements was made at each. The vapor pressures at the three higher temperatures were measured with the external mercury manometer using the 300 mm head as a pressure null detector. Helium was used as the balancing gas.

The data of Fisher and McMillan[41] were used to relate the vapor pressure data at the lowest temperature to the Kelvin temperature scale, while that of Beaumont, Chihara, and Morrison[42] were used at the three higher temperatures. The authors did not indicate the specific temperature scales employed.

The calibration data obtained were fit to a third order polynomial using a least squares program on a Wang 700A electronic calculator. The goodness of the fit of the polynomial to the data was well within the experimental error. The results appear in Table 1.

The uncertainty in the EMF measurements was the equivalent of about $0.05^{\circ}K$ over this temperature range. Also the uncertainty in the vapor pressure measurements resulted in approximately the same uncertainty in the temperature; consequently, the thermocouple calibration was taken to be accurate to within $\pm 0.1^{\circ}K$.

The potentials of the five remaining thermocouples were determined at the boiling point of distilled water, and the conversion relations found in the International Critical Tables were used to convert the observed thermocouple EMF's to degrees centigrade. The temperatures thus found agreed to within $\pm 1^{\circ}C$ with the temperature of boiling water at the ambient pressure. This agreement was considered sufficient and the conversion relations were accepted as the calibration for these thermocouples.

Volume Calibration

In order to carry out the volumetic adsorption experiment, the dose volume and the volume of the space occupied by the adsorbate after expanding the dose had to be known. In fact, these two volumes were further subdivided because of temperature variations within each. Figure 8 indicates the division of the system's volumes and Table 2 gives the values

Table 1. Cryostat Thermocouple Conversion Relations
($77^{\circ}K < T < 109^{\circ}K$)

$T(^{\circ}K) = A_3(EMF)^3 + A_2(EMF)^2 + A_1(EMF) + A_0$				
Thermo-couple Number	A_3	A_2	A_1	A_0
6	20.361	308.91	1616.5	3003.0
7	16.410	246.59	1288.0	2429.7
8	18.047	272.52	1424.8	2670.1
EMF in millivolts				

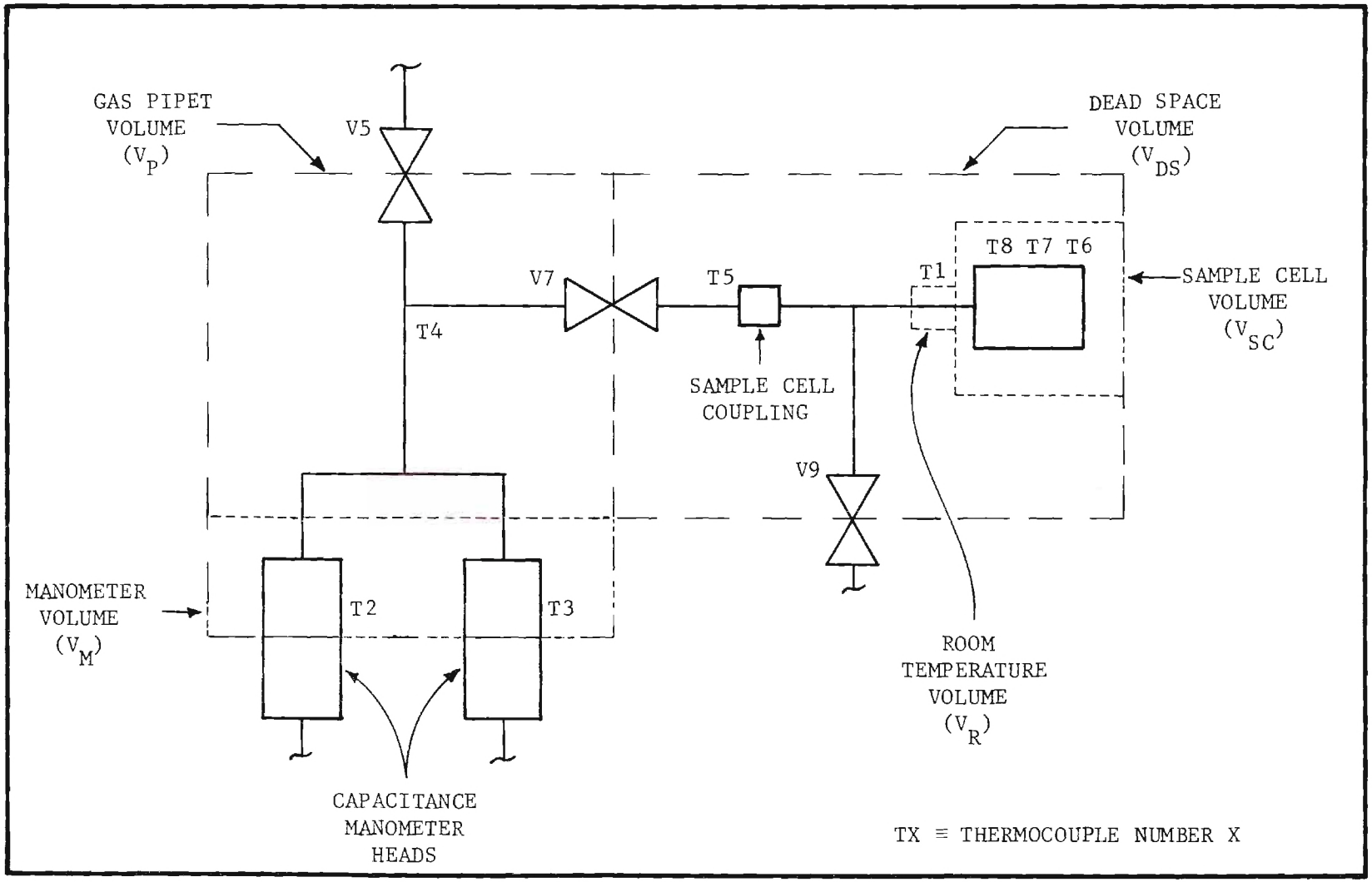

Figure 8. Division of the Apparatus' Volume for Calibrations

Table 2. Calibrated Volumes

VALUES OF THE VOLUMES IN THE ADSORPTION APPARATUS	
Volume Designation	Value (cm^3)
Primary Calibrated Volume (PCV)	42.231 ± 0.003
Gas Pipet Volume (V_p)	24.25 ± 0.2
Dead Space Volume (V_{DS})*	32.41 ± 0.4
Sample Cell Volume (V_{SC})*	15.09 ± 0.3
Tubing in Room (V_r)	1.57 ± 0.3
Manometer Volume (V_m)	8.90 ± 0.3
Copper Sample Volume	1.84 ± 0.005
*Copper sample in cell	

of the volumes as found during the calibration procedure.

The required volumes were found by expanding helium and applying the ideal gas law. A more accurate method such as mercury displacement would have been preferred, but because of the cleanliness requirement of the experiment and the nature of certain components of the vacuum system, only a gas expansion technique could be used.

The first step in the calibration procedure was to prepare a gas pipet with an accurately known volume (Figure 9). The volume of the pipet was found in the following way: A vacuum line with a Fisher-Porter valve as throttle was attached to pipet's stopcock and mercury was pulled from a reservoir into the pipet, which was constantly tapped with a wooden rod to prevent bubble formation along its walls. The mercury level was raised until the stopcock had been filled. The stopcock was closed and the pipet was inverted. The mercury level in the capillary was carefully lowered by opening the stopcock until the mercury meniscus was a few millimeters below the fiducial. The mercury-filled pipet was placed in a constant temperature air bath and allowed to equilibrate for five hours while the EMF of a thermocouple taped to the pipet was monitored. At the end of this period the position of the mercury in the capillary was determined with respect to the fiducial and the pipet was removed from the bath. The mercury was very carefully drained into a previously weighed flask and the mass of mercury present was determined using a Mettler Kilogram Balance (Serial No. 45736). An estimate of the volume of the mercury was obtained from the density of mercury[43] at the air bath temperature and this volume was used to correct the observed mass for the displacement of air by the mercury. A final volume was then calculated

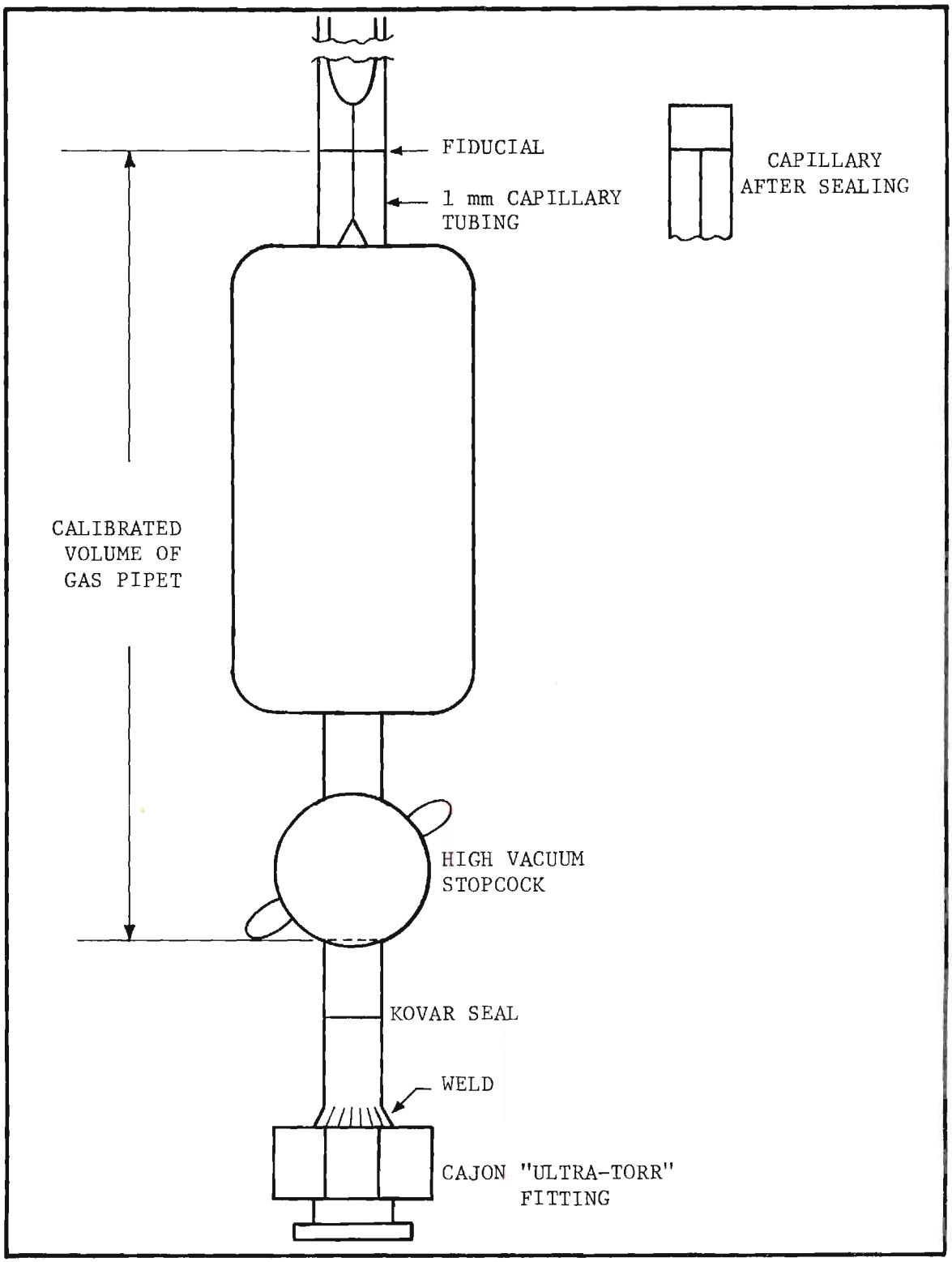

Figure 9. Removable Calibrated Volume

as above but using the corrected mass of mercury.

The pipet's stopcock was disassembled, cleaned, and reassembled and the entire procedure was repeated. The second determination indicated a volume which was within 0.002 cm^3 of that of the first determination.

The stopcock was again disassembled and the pipet was cleaned with nitric acid to remove any trace of mercury which remained and the capillary was sealed at the fiducial. A pyrex to kovar seal was blown onto the stopcock and a 1/4 in. Cajon (4 VCR) ultra-high vacuum fitting was arc welded to the kovar.

The gas pipet was attached to the adsorption system in place of the sample cell line and relabeled the primary calibrated volume or PCV.

In order to carry out the gas expansions with the greatest possible accuracy, a mercury U-tube manometer was attached to the reference side of the capacitance manometer system. The mercury manometer was isolated from the ultra-high vacuum system by two large traps kept at dry ice temperature. The mercury columns were of sufficient diameter to effectively prevent capillary depression, and the density of the mercury was corrected to $0^{\circ}C$ in calculating the pressures. In all of the measurements helium was bled into the mercury manometer system until the capacitance manometer indicated a zero pressure differential. The heights of the mercury columns were determined with a cathetometer (Gartner Scientific, College Model) and the pressure calculated from these data was considered the pressure in the adsorption system.

In the first set of experiments, a known quantity of gas was expanded from the adsorption system into the PCV. This allowed the determination of the volume of the adsorption system up to the stopcock of the PCV.

Next a known quantity of gas was expanded from the gas pipet into the remainder of the adsorption system up to the PCV stopcock. This gave the volume of the gas pipet. Normally the capacitance manometer heads were held at 40°C in order to improve the zero stability. Since this was about 10 degrees above the temperature of the remainder of the gas pipet, this volume was further subdivided into a volume in the manometer heads (V_m) and the remainder of the volume of the gas pipet. The volume of the manometer heads was obtained from values provided by the manufacturer.

The PCV was removed at this point and the sample cell was attached. Known amounts of helium were expanded from the gas pipet into the sample cell. These expansions were carried out with the sample cell at room temperature (299°K), 81°K, and 84°K. The room temperature data allowed the determination of the total volume of the adsorption system outside of the gas pipet and all three sets of data taken together allowed the calculation of the effective volume of the sample cell.

A short length of the sample cell tubing ran between the oven and the cryostat and consequently was approximately at room temperature. The volume (V_r) of this tubing was calculated from its length and an assumed uniform inside diameter of 1/16 in.

Finally the volume of the copper sample had to be taken into account. This was done by weighing the sample on a Mettler Analytical balance and computing the volume of copper from its density. The density of copper used was 8.92 g/cm^3.

Capacitance Manometer Calibration

The two MKS "Baratron" manometer heads used in the apparatus had

rather different characteristics, consequently their calibrations were handled differently. The manufacturer indicated that the sensitivity of the 90H-300 head tended to change with time while that of the 90H-1 head was extremely constant (varying less than 0.1% over a period of 500 hours at 150°C). As a result the calibration of the 90H-300 head was occasionally checked against the external mercury manometer while the manufacturer's calibration of the 90H-1 head was accepted and used throughout the experiments described here.

Generally when critical pressure measurements in the range of the 90H-300 head had to be made, the head was used only as a null detector for the external mercury manometer. The calibration of the head was periodically checked against the mercury manometer, however, and the calibration supplied by the manufacturer was always found to be very close to that observed.

The manufacturer used the following procedure in calibrating the 90H-1 head[44]. The capacitance manometer system was calibrated as a unit, i.e., the particular readout furnished with the head was used during the calibration. The calibration set up is shown in Figure 10. The 'zero' of the 90H-1 unit was set with no pressure differential across the diaphragm (valves V_2 and V_3 open). With valves V_2 and V_3 closed the cylinders of both dead weight testers (DWT) were floated and the weight on the reference DWT was adjusted so that the manometer again read zero. Weights were then added to the calibrating DWT in increments equivalent to 0.10000 torr until a total pressure of 1 torr had been reached. The manometer reading at each step was recorded thus resulting in a calibration for the head. The weights used in the calibration were traceable to the National

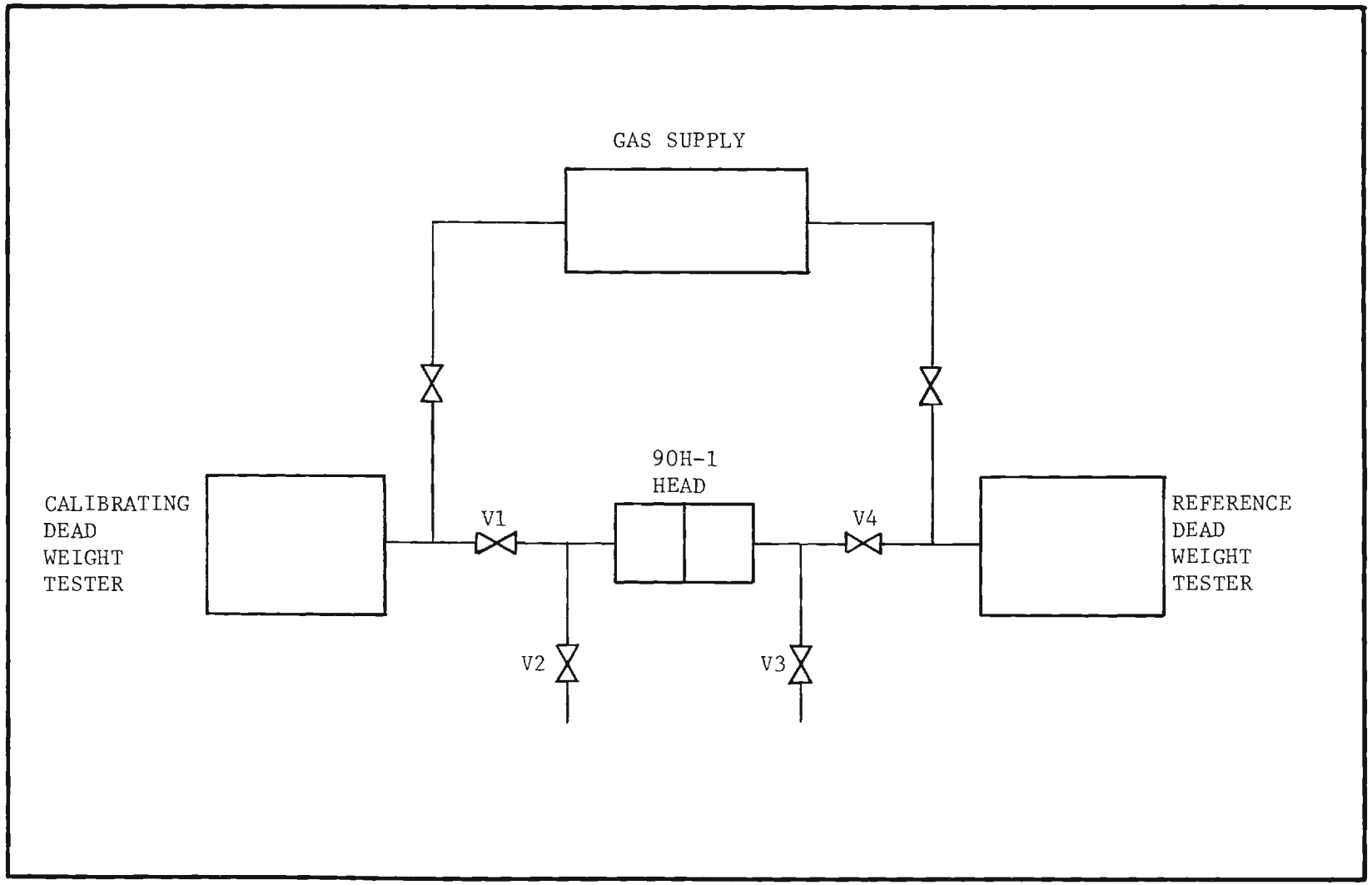

Figure 10. Capacitance Manometer Calibration Setup

Bureau of Standards.

A very stable capacitance manometer such as the 90H-1 is capable of more accurate pressure measurements than a McLeod guage[45]. The precision and accuracy of pressure measurements made with the 90H-1 head are given in Table 3.

Table 3. Uncertainty in the Capacitance Manometer Measurements

Pressure (Torr)	Uncertainty In Pressure (Torr)
0.00005	±0.000005
0.0001	±0.000005
0.001	±0.00002
0.01	±0.00005
0.1	±0.0003
1	±0.001

CHAPTER III

EXPERIMENTAL PROCEDURES AND DATA TREATMENT

Isotherm Procedures

The isotherm data which are reported here were obtained by following procedures summarized below.

Sample History

The copper single crystals which constituted the adsorbate in this study were grown, polished, and characterized by McAlpin[37]. At the conclusion of the experiments conducted by McAlpin, the surfaces of the crystals appeared to be suitable for further adsorption studies. As a result they were placed in an evacuated container for storage. When the current adsorption apparatus was deemed ready for the measurements to commence, the crystals were removed from the container and inspected both macroscopically and microscopically with a Carl Zeiss Standard Metallurgical Microscope. The color, brightness, and texture of the surfaces indicated that the sample had not deteriorated perceptibly during the period of storage. While the possibility of chemical contamination of the surfaces could not be ruled out, it was felt that any contaminant which might be present would be removed by the high temperature bakeout or the hydrogen reduction of the sample prior to the isotherm measurements. Because of these considerations and the high crystal loss rate associated with the electropolishing technique which would have been required for further surface preparation, it was decided to carry out the measurements on the sample without further treatment.

Insertion of the Sample Into the Apparatus

The study of the adsorbent was begun by loading the crystals into the freshly electropolished nickel sample cell. The sample was suspended in the cell from a 1/16 in. diameter rod (99.999+ percent copper) which had been slotted to maintain the separation of the crystals.

A preformed vacuum annealed copper gasket was then slid over the sealing surface of the sample cell top. The top was aligned with the body of the cell and the eight bolts used to pull the sealing surfaces together were placed in the bolt circle and the nuts were run up to finger tightness. The work required to form a dependable seal by tightening these bolts was very great and the sample cell was occasionally jarred severely in the process. With the sample in the cell this had to be avoided. For this purpose a special vise was built which held the lower part of the cell securely while the bolts were tightened. When it was felt that a dependable seal had been obtained, a mass spectrometer leak detector (Veeco model MS9AB) was used to search for real leaks. If none were found as was normally the case, the cell was subjected to an extensive bakeout. For the data reported here the sample cell had to be sealed twice, once before the copper series of isotherms and again before the sample cell series.

After the system had been exposed to atmospheric gases and other contaminants as it was during the sample loading or removal phases, it had to be outgassed extensively to obtain pressures in the ultra-high vacuum range. The sample cell was baked at 300° C for a period of approximately a week. Various other portions of the system were heated either with a hot air blower or a soft torch flame. The capability existed for

baking the entire vacuum system at approximately 300° C, but this was not done because such a procedure caused problems with various components of the system. It was observed that localized baking and pumping for a period of approximately a week produced the same ultimate pressure as a ten hour bake at 300° C. The time lost was considered insignificant relative to the instrumental problems which resulted from a general bakeout.

Hydrogen Reduction of the Sample

When the pressure in the system had fallen to 5×10^{-8} torr the reduction treatment began. The purpose of this treatment was to produce a copper surface free of any oxide which might have formed during exposure to air or residual oxygen in the vacuum system.

The sample cell was heated to 460° ± 10° C. An iron-constantan thermocouple was used to monitor the temperature during this phase. When the temperature had become stable, valves 7 and 9 (Figure 3) were closed. Assayed Reagent grade hydrogen was expanded from the chemical manifold with its trap at liquid nitrogen temperature into the gas pipet. Valve 7 was opened and the pressure was followed with the 90H-300 manometer head. When the pressure became stable (approximately 1/2 min.), valve 7 was closed. The hydrogen was allowed to reside in the sample cell for 10 minutes. Valve 9 was opened and the hydrogen and any water vapor formed were pumped out. Valve 9 was closed after 5 minutes and another dose of hydrogen was admitted. This process was iterated for a total of 10 treatments. The hydrogen pressure in the sample cell during the reduction treatment varied from 150 to 250 torr.

Normally at the end of the reduction treatment the pressure in the vacuum system was in the high 10^{-7} torr range. The sample cell oven was

left at the temperature of the reduction and the system was pumped out for a period of from 3 to 5 days. Various portions of the system were again baked with the hot air blower or a torch. During this period the system pressure fell below 5×10^{-8} torr. The system was now ready for the isotherm measurements.

Isotherm Measurement

Beginning the isotherm measurements required that the adsorption apparatus be prepared and the cryostat set in operation at the same time. These two operations will be described concurrently as they occurred in the experiment.

Approximately one hour after the sample cell bakeout had ended, the bakeout furnace was removed. The sample cell was properly positioned in the cryostat and three thermocouples were attached to it. Thermocouple number 8 was taped to the sample tube just at the position of the top of the liquid nitrogen bath. Thermocouple number 7 was taped to the sample cell just below its flange and thermocouple number 6 was taped to the lower edge of the sample cell. The cryostat tank was then brought up, sealed, and the external insulation was applied.

The capacitance manometer electronics were checked and the zero of the 90H-1 head was adjusted. Valves 5 and 9 were closed and the output of the manometer on the 0.001 torr scale was recorded on the strip chart recorder. Valves 6 and 8 were opened in order to pump out the chemical manifold.

The vapor pressure thermometer in the cryostat was filled with argon or krypton depending on the temperature of the isotherm to be studied. A 160 liter pressurized dewar of high purity liquid nitorgen was attached

to the condenser filling system, and a "standard" cylinder of compressed prepurified grade nitrogen was attached to the cryostat filling system. A low flow of nitrogen gas was established through the filling system to remove any water vapor present. The cryostat bath was filled with liquid nitrogen from a 25 liter storage dewar. While the bath was filling the condenser level controlling system was switched "on" thus filling the condenser dewar with liquid nitrogen. When the cryostat bath had filled, the bath level controlling system was started in operation. At this point the cryostatic bath had been established and the systems required to maintain it were in operation. Next the desired temperature for the isotherm had to be obtained.

The filling port was sealed and all of the valves controlling the escape of gas from the cryostat were closed. The pressure in the cryostat, followed with a Bourdon gauge, was allowed to rise until it had reached the vapor pressure of nitorgen at the desired temperature. The exit valves were adjusted so that this pressure was maintained. The mercury level in the manostat was adjusted until it was just below the tip of one of the lower contacts. This was achieved by carefully adjusting the pressure on the reference side of the manostat. The automatic temperature regulating system was activated and the bath was allowed to come to "equilibrium." The EMF's of the three thermocouples in the bath were measured to be certain that the desired bath temperature had been obtained. If this was not the case, the pressure on the reference side of the manostat was adjusted in such a way as to bring the bath temperature closer to the desired value. When the desired temperature had been achieved, the cryostat was ready for the isotherm measurements to commence.

The operation of the cryostat from this point was controlled automatically except for an occasional tuning of the filling or gas escape rates or the replacing of an expended nitrogen cylinder.

With the desired temperature established in the cryostat, the next step was to be certain that the copper sample was also at this temperature by expanding helium into the sample cell. With valves 6, 7, 8, and 9 closed, analyzed reagent grade helium (Air Reduction Sales Company) was expanded into the chemical manifold which was trapped at liquid nitrogen temperature. Valve 6 was opened carefully and the helium pressure in the gas pipet was allowed to rise to 0.4 torr. Valve 5 was closed and valve 7 opened allowing the helium to expand into the sample cell. This procedure provided a pressure of approximately 0.2 torr of helium in the cell. Valve 8 was opened and the helium remaining in the chemical manifold was pumped out. The pressure of the helium in the sample cell was monitored and when it had become constant (approx. 30 min.) valve 9 was opened thus pumping the helium out of the system. The helium pump out continued for an hour during which the pressure again fell to the 10^{-8} torr range. Valve 9 was then closed and the 90H-1 manometer head output was recorded for 1 to 1 1/2 hours while any helium which had been trapped in the cell found its way into the system and the true background pressure could be determined. At the end of this period the adsorption system was ready for the isotherm measurements to begin.

Valves 5, 6, 7, and 8 were again closed. Assayed reagent grade krypton (Air Reduction Sales Company) was expanded into the chemical manifold which was now trapped with "dry ice." Valve 6 was cracked open and a small amount of krypton was allowed to expand into the volume

between valves 5, 6, and 8. Valve 5 was cracked open and the first dose was expanded into the gas pipet. The dose was allowed to reside in the pipet until its pressure had become constant thus indicating thermal equilibrium had obtained. The dose pressure was recorded on the strip chart recorder and valve 7 was opened allowing the krypton to enter the sample cell. Usually 1/4 hour was required for equilibrium to be established in the system. When the pressure again became constant the equilibrium pressure was recorded with the dose pressure, as were the EMF's of all of the thermocouples in the system. The dosing procedure was continued until the equilibrium pressure was approaching the 1 torr limit of the 90H-1 head. Unfortunately, the precision of the 90H-300 head was far below that required in the experiment, thus 1 torr represented the upper limit of the useful pressure measuring capacity of the system.

Four isotherms were determined in accordance with the above procedures. The copper crystals were then removed from the sample cell and four more isotherms were determined at the same temperatures as the previous isotherms. The procedures followed in determining the second set of isotherms were identical to those set forth above except the crystals were not in the sample cell.

Treatment of the Raw Experimental Data

The data collected for each point observed during an experiment consisted of a dose pressure P_d, an equilibrium pressure P_e, and a set of EMF measurements which gave the temperatures of the volumes containing the krypton. The isotherms were then calculated from these data in the following way.

The idea underlying the calculation was that the difference between

the total amount of krypton introduced into the system and the amount remaining in the vapor phase must be the amount adsorbed. Before deriving the relations indicated, it was necessary to decide which equation of state was best suited to describe the pV behavior of the krypton remaining in the vapor phase. It was found that at the highest krypton density encountered in the experiment, the difference in the number of moles of krypton present in the system calculated using the ideal gas equation of state and the virial equation of state[2] was less than one percent. Consequently the "ideal gas law" was used throughout the data treatment.

The number of moles of krypton introduced into the gas pipet by the i^{th} dose was obtained from

$$N_{di} = \left[P_{di} - P_{e(i-1)}\right]\left(\frac{V_d}{T_d}\right)\left(\frac{1}{R}\right) \tag{39}$$

where P_{di} = the pressure of the i^{th} dose

$P_{e(i-1)}$ = the equilibrium pressure after expanding the $(i-1)^{st}$ dose

R = the gas constant

$$\left(\frac{V_d}{T_d}\right) = \left[\frac{V_p - V_m}{T_o} + \frac{V_m}{T_m}\right]$$

V_m = volume of the capacitance manometer heads = 8.90 cm^3

V_p = volume of gas pipet = 24.25 cm^3

T_o = temperature of oven

T_m = the average of the temperatures of the two manometer heads

The *total amount of* krypton which had been introduced into the system after expanding the i^{th} dose was simply

$$N_{Ti} = \sum_{k=1}^{i} N_{dk} \tag{40}$$

The amount of krypton in the vapor phase after expanding the i^{th} dose was obtained from

$$N_{Vi} = \left\{ P_{ei}\left(\frac{V_d}{T_d}\right) + P_{ei}\left[\left(\frac{V_{ds} - V_{sc} - V_r}{T_o}\right) + \frac{V_r}{T_r}\right] + P_{eci}\left(\frac{V_{sc}}{T_{sc}}\right)\right\}\left(\frac{1}{R}\right) \tag{41}$$

where

V_{ds} = the total volume of the adsorption system outside of the gas pipet

= 34.25 cm^3 without copper crystals in cell

V_{sc} = volume of the sample cell

= 16.93 cm^3 without copper sample in cell

V_r = volume of the adsorption apparatus which was at room temperature

= 1.57 cm^3

P_{eci} = the pressure of the krypton in the sample cell

P_{eci} was found by correcting P_{ei} for thermal transpiration between the hot and cold regions of the system using the method developed by Miller[46].

The amount of gas absorbed when equilibrium obtained after the i^{th} dose was then found from

$$N_{ai} = N_{Ti} - N_{Vi} . \tag{42}$$

The set of equilibrium pressures in the sample cell (P_{eci}) and the corresponding amounts of gas adsorbed (N_{ai}) constitutes the isotherms reported here.

Some refinements of the experimental data were required before they could be used in the above relations. Two corrections were made to the pressure data.

First, the 90H-1 capacitance manometer output was slightly nonlinear with respect to pressure. To obtain the correct pressure from a manometer reading a small correction supplied by the manufacturer had to be applied. Second, despite the long bakeout after the hydrogen treatment and the pumpout after the helium cooling stage there was always a measurable residual pressure of hydrogen and helium in the sample cell at the beginning of an isotherm determination. The pressure of these residual gases was observed to increase rapidly when the sample cell region was sealed just prior to the beginning of an isotherm determination. Within one hour, however, the pressure was usually increasing at a rate of 0.00003 torr/hr. or less. The residual gases were generally a significant fraction of the vapor present for the first few points observed during an isotherm determination, and they were taken into account by observing their build up, prior to admitting any krypton, until the rate became constant. With this information the partial pressure of the residual gases present could be calculated for any time during the

isotherm determination and subtracted from the total pressure observed in order to obtain the pressure of the krypton present.

The data obtained from the thermocouples were converted to the Kelvin temperature scale using the conversions indicated in Chapter II. There were a total of 8 thermocouples in the system and they were combined as follows:

$$T_{sc} = \frac{T_6 + T_7 + T_8}{3}$$

$$T_o = \frac{T_4 + T_5}{2}$$

$$T_M = \frac{T_2 + T_3}{2}$$

$$T_r = T_1$$

where the numeral subscript indicates the thermocouple from which the temperature measurement was obtained.

The maximum possible error associated with each isotherm point was calculated in the following way. The maximum uncertainties in the P_{ei} and P_{di} were found by assuming the largest error consistent with the precision indicated by the manufacturer for the 1 mm capacitance manometer head (Table 3). The uncertainty in P_{ei} was subtracted from its value, and the uncertainty in P_{di} was added to its value thus forming a new set of pressure data. The correction for residual gas pressure was increased by 20 percent and the isotherms were recalculated as above. The difference between a point on one of these constructed isotherms and the corresponding point on the experimental isotherm was taken as one-half

of the maximum uncertainty in the experimental point. It was observed that reasonable variations in the temperatures produced no significant changes in the isotherm points.

The low level of scatter relative to the calculated uncertainties would seem to imply that the random errors are much smaller than the limits indicated. Errors involved in this type of calculation are cumulative, however, and smoothness of the isotherm cannot be taken as an indication of the precision of the pressure measurements involved.

The final step in the reduction of the experimental data was the calculation of the amount of krypton absorbed on the copper single crystals, i.e., the construction of the copper-krypton isotherms. Because of the experimental set-up, the measurements always involved some adsorption on the sample cell walls as well as the copper crystals. In fact, the area of the exposed sample cell walls was roughly comparable to that of the copper sample; consequently, the krypton adsorbed on the cell walls always represented a significant fraction of the total amount adsorbed.

The correction for the amount adsorbed on the cell walls was made in the following way. As indicated above, a pair of isotherms was determined at each temperature studied. One isotherm was measured with and the other without the sample in the cell. The isotherms without the sample in the cell were plotted on a scale which introduced no additional uncertainty and smooth curves were drawn through the points. Thus four continuous isotherms were obtained. These isotherms were used to determine the amount of krypton adsorbed on the cell for each point in the isotherms measured with the sample in the cell. The sets of points obtained by

subtracting the amount adsorbed on the cell from the total amount adsorbed on the cell and sample were taken as the copper-krypton isotherms.

The copper-krypton isotherms are tabulated in Appendix A. The uncertainties given there were obtained by summing the uncertainties in the appropriate experimental isotherms.

CHAPTER IV

DATA TREATMENT AND RESULTS

A total of eight isotherms were measured during the course of the experiments thus allowing calculation of four copper-krypton isotherms. The temperatures of these isotherms were 78.86, 91.17, 98.64, and 107.96 degrees Kelvin. The isotherm data are tabulated in Appendix A and plotted in Figure 11. This chapter describes the information about the copper-krypton system extracted from these isotherms.

Surface Area of the Crystals

A photographic technique was used to determine the geometric area of the copper crystals. The crystals were placed on a piece of paper ruled into 1 mm^2 sections, and the crystals and grid were photographed. An enlargement was made and used to determine the number of sections covered by the crystals. This procedure gave an area of 68.6 cm^2 for the (1,1,1) plane of copper (broad faces) exposed to the adsorbate. The total circumference of the crystals was determined from the enlargement and 0.1 cm was taken as the average thickness of the crystals resulting in an edge area of 10.0 cm^2. Consequently, the total geometric area of the sample was 78.6 ± 2 cm^2.

The BET area of the copper crystals was determined by plotting the 79°K isotherm data according to the scheme suggested by equation (38). Only those points for which $3 \times 10^{-3} < X < 5 \times 10^{-2}$ were used and the resulting curve was indeed a straight line. The monolayer volume (V_m)

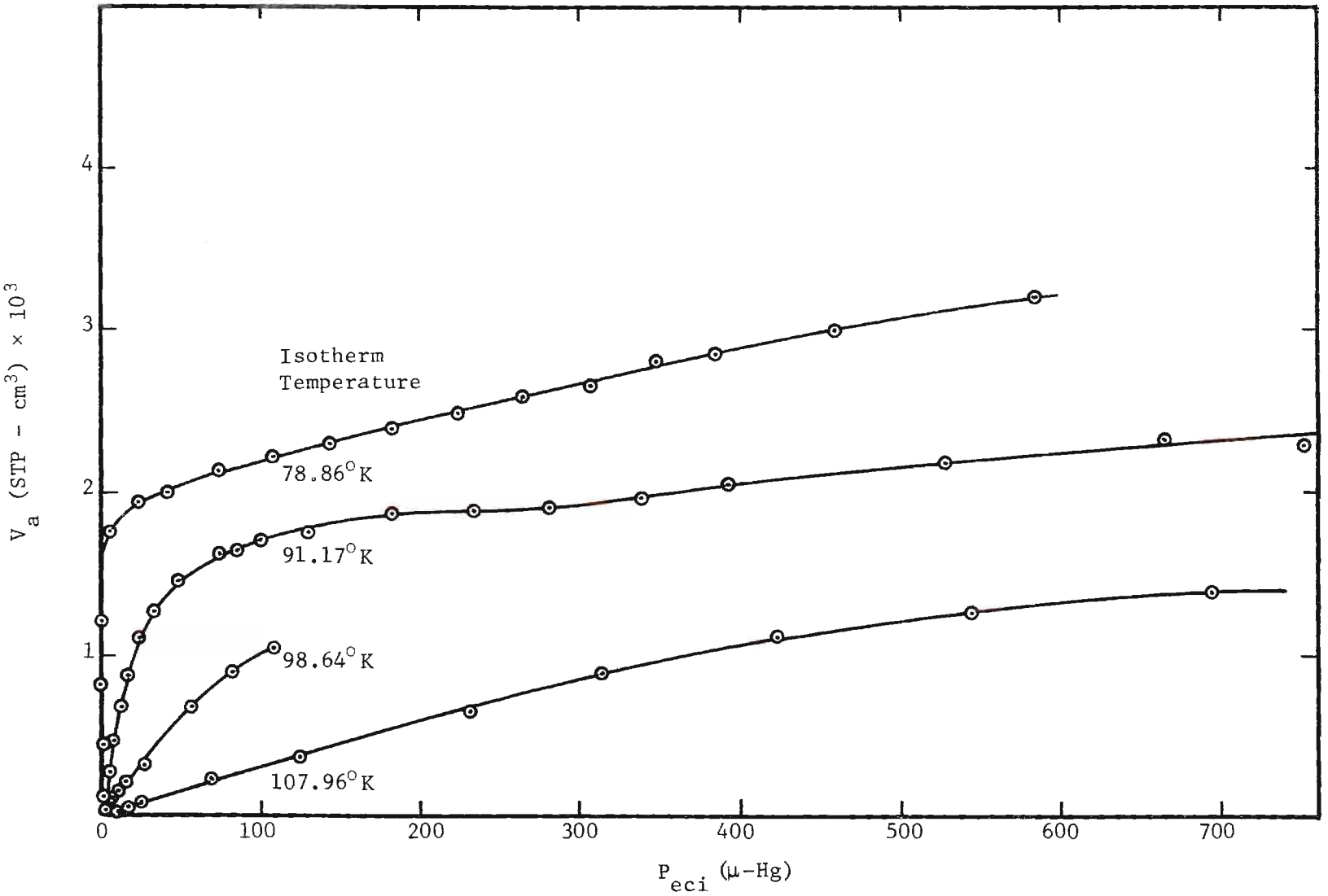

Figure 11. Experimental Copper-Krypton Isotherms

determined from the plot was 2.20×10^{-3} STP-cm^3. By assuming an area of 19.5 $\AA^2$ per atom of krypton, the surface area of the sample was calculated to be 115 cm^2.

The area determination gave the roughness factor, defined as the BET area divided by the geometric area, of the copper crystals as 1.46 which is within the range normally observed for highly polished copper crystals.[22]

This same procedure applied to the 79°K sample cell isotherm gave a roughness factor of 7.8 for the cell. The very bright and smooth appearance of the interior of the nickel cell indicated that this high roughness factor could not be due to roughness of the walls of the cell. Instead it was felt that oxidation of the unpolished surface of the interior of the stainless steel tubing leading into the sample cell was responsible. This assumption required that the roughness factor of the tubing be very high since the geometric area of the cold portion of the tubing represented only about 10 percent of the total area of the sample cell.

Table 4. The Surface Areas of the Sample and the Sample Cell.

	Copper	Sample Cell
Geometric Area (cm^2)	78.6 ± 2	49.5 ± 3
BET Area (cm^2)	115	390
Roughness Factor	1.46	7.8

Virial Analysis

The virial equation of state (Equation 11) offers a very attractive means of interpreting low coverage physical adsorption data. Two aspects of the theory require consideration, however, before proceeding to make use of it here.

First, the power series in the fugacity as given in Equation (11) contains the coefficients which are directly related to the intermolecular forces of interest. However, in applying the theory to experimental data, it is more convenient to use an expansion in the pressure. If this is done, interactions in the gas phase must be taken into account.

The virial equation in the pressure is usually written, after Halsey,

$$N_a = B_{AS}\left(\frac{P}{RT}\right) + C_{AAS}\left(\frac{P}{RT}\right)^2 + \cdots \quad . \tag{43}$$

If the equation of state of the gas phase is also written as a virial expansion, the first two coefficients of equations (11) and (43) are related as follows:

$$B_{AS} = B_{2,S}$$

$$C_{AAS} = B_{3,S} + B_{2,S}B^{o}_{2,g}$$

where $B^{o}_{2,g}$ is the second virial coefficient of the gas.

Under the conditions of these experiments,

$$\frac{B_{3,S}}{B_{2,S}B^{o}_{2,g}} \geq 1{,}000 \quad ,$$

consequently, the first two coefficients of the two series are effectively equal. Henceforth the $B_{(i+1),S}$ notation will be used even though the experimental coefficients result from an expansion in the pressure.

The second and less trivial point concerns the choice of a technique for obtaining the desired virial coefficients from the isotherm data. One method is to computer fit the isotherm data to a polynomial and equate the resulting coefficients to the virial coefficients of corresponding powers of the pressure. The method of Sams, Constabaris, and Halsey[32] was chosen to be used here, however, because it gives the true zero pressure limit virial coefficients as well as an insight into the uncertainty in the coefficients obtained from the fitting technique.

With the pressure substituted for the fugacity, equation (11) reads

$$N_a = B_{2,S}\left(\frac{P}{RT}\right) + B_{3,S}\left(\frac{P}{RT}\right)^2 + \ldots . \tag{44}$$

Equation (44) can be rearranged to give

$$\frac{N_a RT}{P} = B_{2,S} + B_{3,S}\left(\frac{P}{RT}\right) + \ldots . \tag{45}$$

Consequently,

$$B_{2,S} = \lim_{P \to 0}\left(\frac{N_a RT}{P}\right) . \tag{46}$$

Equation (46) indicates that $B_{2,S}$ is the intercept of a plot of $\frac{N_a RT}{P}$ versus P. Similarly

$$B_{3,S} = \lim_{P \to 0} \frac{\left(\frac{N_a RT}{P} - B_{2,S} \right) RT}{P} \quad . \tag{47}$$

Equations (46) and (47) give the proper methods for relating the isotherm data to the coefficients of the virial expansion.

A plot of $\frac{N_{ai}RT}{P_{eci}}$ versus P_{eci} of the low coverage data from the 91°K isotherm is shown in Figure 12. This figure illustrates two of the major problems encountered in applying the virial equation to physical adsorption data. The rapidly increasing error limits as the pressure decreases indicate the sensitivity of the plot to errors in the experimental data. This is particularly important because the lowest pressure points contain the information required for a valid extrapolation to zero pressure. Also, if the isotherm itself does not extrapolate to $N_a = 0$ at $P = 0$, the $B_{2,S}$ plot will approach zero pressure asymptotically. The upward curvature of the low pressure points may be a result of this effect. While it is possible to make these problems appear less severe by using other fitting techniques, the resulting virial coefficients have no more physical significance than those obtained by this method.

The low coverage data from the 99 and 108°K isotherms were plotted in the same manner. The 79°K isotherm was not treated because the lowest coverages observed were too great for the virial equation to apply. The results of plotting these two isotherms were quantitatively similar to Figure 12. This result suggests two methods of carrying out the required extrapolation to zero pressure. The lower pressure points, corresponding to those lying along line A in Figure 12 could be extrapolated without

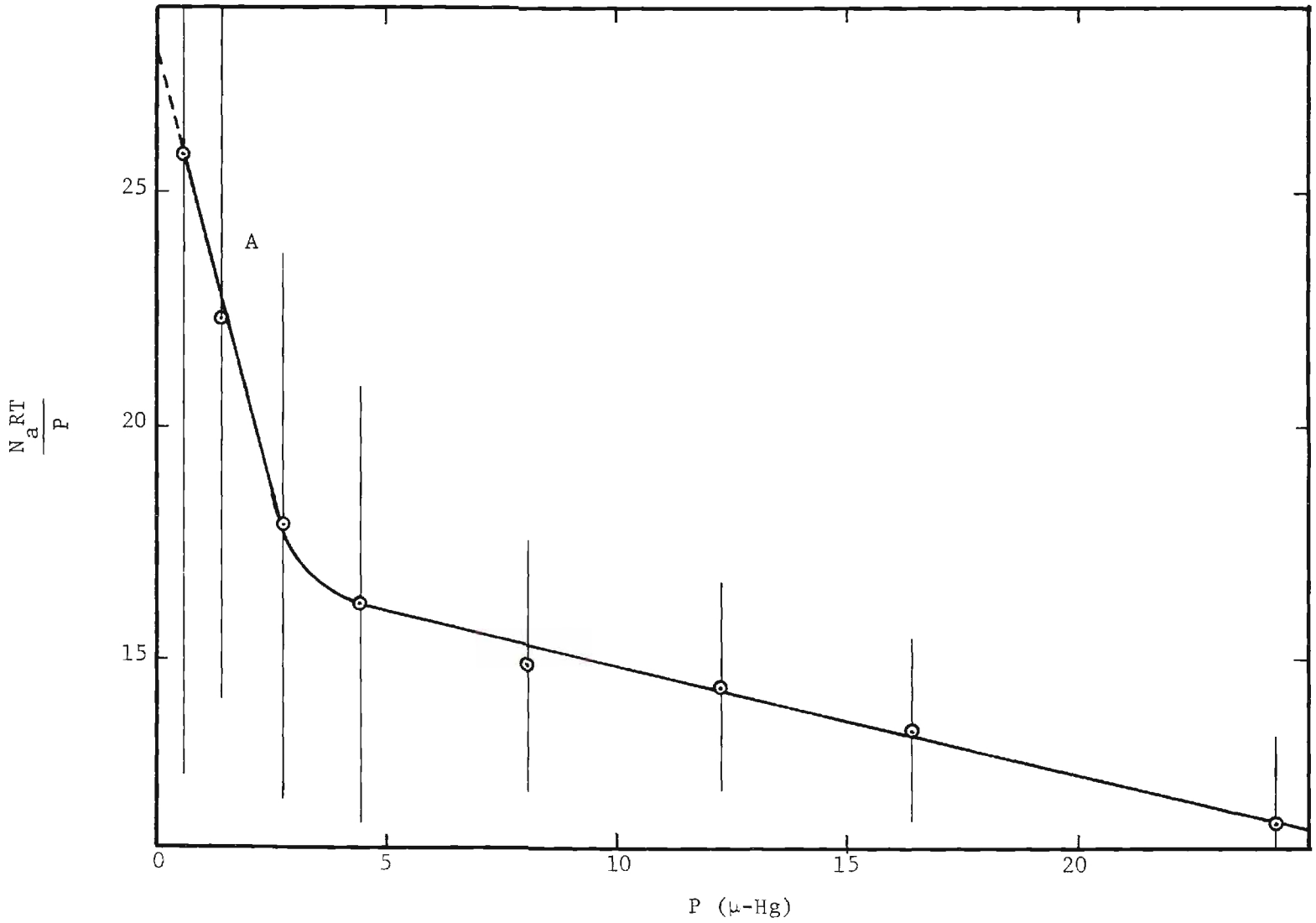

Figure 12. Virial Plot of the Low Coverage 91°K Isotherm Data

regard to the higher pressure points or the higher pressure points could be used and the lower pressure points neglected. The physical significance of these two possibilities are considered later. First, the two sets of virial coefficients corresponding to the different methods of extrapolating to zero pressure are found and analyzed to give $\epsilon^*_{1,S}$, the minimum in the gas-solid interaction potential, and A, the area of the sample.

The virial coefficients from extrapolating the lower pressure points were determined by finding the intercept of the best straight line through the points as determined by a least squares fit. For the 91°K isotherm this was equivalent to extrapolating along line A of Figure 12. The resulting coefficients are given in Table 5.

The virial coefficients corresponding to an extrapolation which neglects the lower pressure isotherm points cannot be found directly from a plot such as that of Figure 12. Figure 13 shows the lower coverage region of the 91°K isotherm. The dashed line indicates a linear extrapolation of the higher pressure points to zero pressure. If this extrapolation is taken as the isotherm, a finite amount of krypton is adsorbed at zero pressure. The virial expansion cannot represent this isotherm because of the non-zero intercept. Instead, an equation of the form

$$N_a = N^\circ + B'_{2,S}\left(\frac{P}{RT}\right) + B'_{3,S}\left(\frac{P}{RT}\right)^2 + \ldots \qquad (48)$$

describes the isotherm where N° is the non-zero intercept. Equation (46) can not be used to obtain $B_{2,S}$ for such an isotherm because

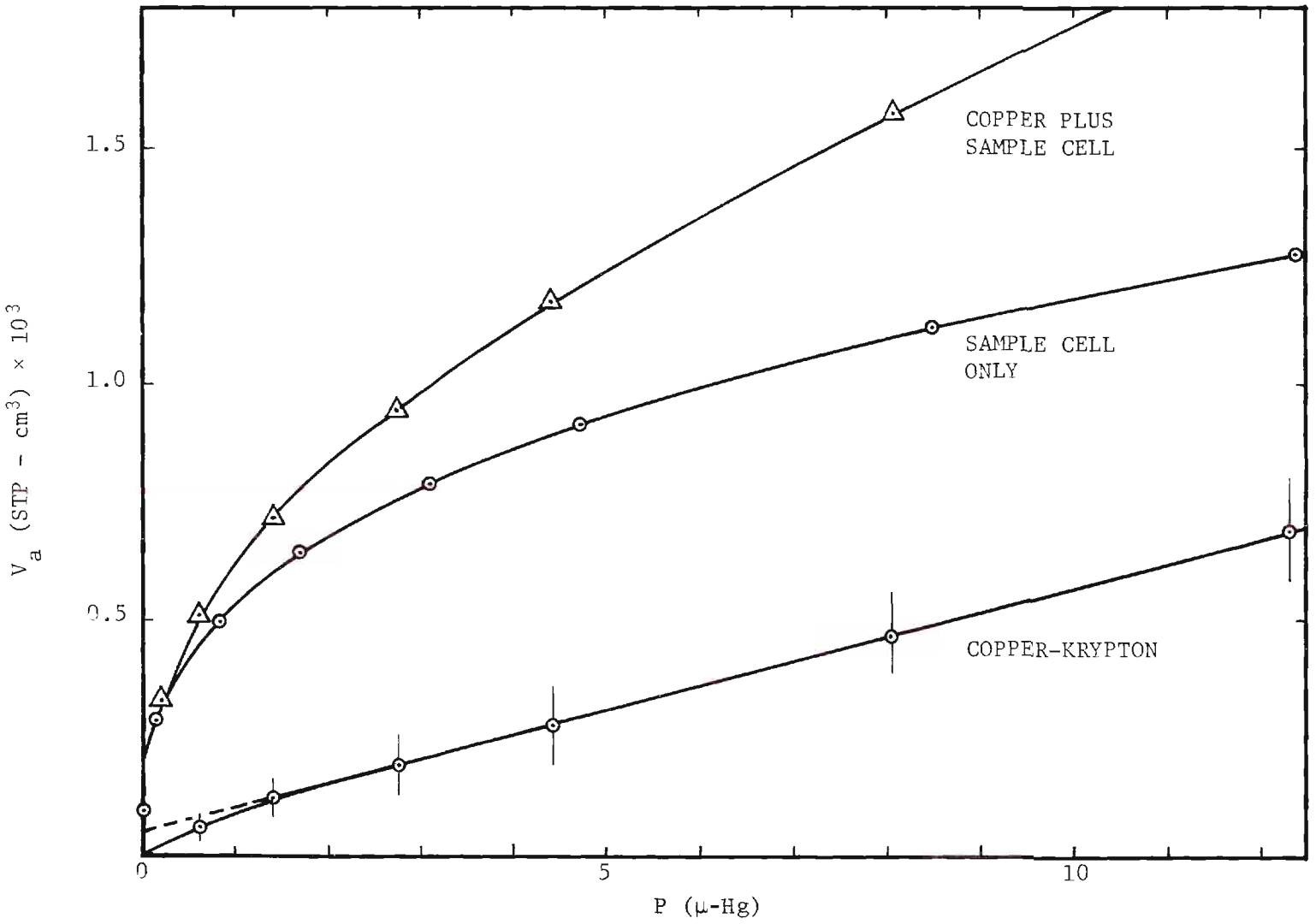

Figure 13. Low Coverage Region of the 91°K Isotherm

$$\lim_{P\to 0}\left[\frac{N_a RT}{P}\right] = \lim_{P\to 0}\left(\frac{N^{\circ}RT}{P}\right) + B_{2,S} = \infty . \tag{49}$$

An effective virial coefficient, $B'_{2,S}$, may be defined as

$$B'_{2,S} = \lim_{P\to 0}\left[\frac{(N_a - N^{\circ})RT}{P}\right] . \tag{50}$$

Figure 14 shows a plot of the $\frac{(N_a - N^{\circ})RT}{P}$ versus P for the lower coverage points of the 91°K isotherm. Taking the non-zero intercept into account simplifies the plot and allows a linear extrapolation to zero pressure.

Finally a method must be found for determining the values of N°. Obviously, the isotherms could be extrapolated as in Figure 13 and the intercept taken as N°. However, a more sensitive method[47] and the one used here is to determine by trial and error the value of N° which most nearly linearizes the lower coverage points of the $\frac{(N_a - N^{\circ})RT}{P}$ versus P plot.

The three isotherms were plotted according to equation (50) and the resulting coefficients are given in Table 5 along with the values of N° used in the calculations.

Table 5. Experimental Values of the Second Virial Coefficients and Non-Zero Intercepts

Isotherm	$B_{2,S}$ (cm^3)	$B'_{2,S}$ (cm^3)	N° (STP - cm^3) x 10^3
91.17	28.3	13.2	0.05
98.64	5.66	3.22	0.025
107.96	1.20	0.932	0.012

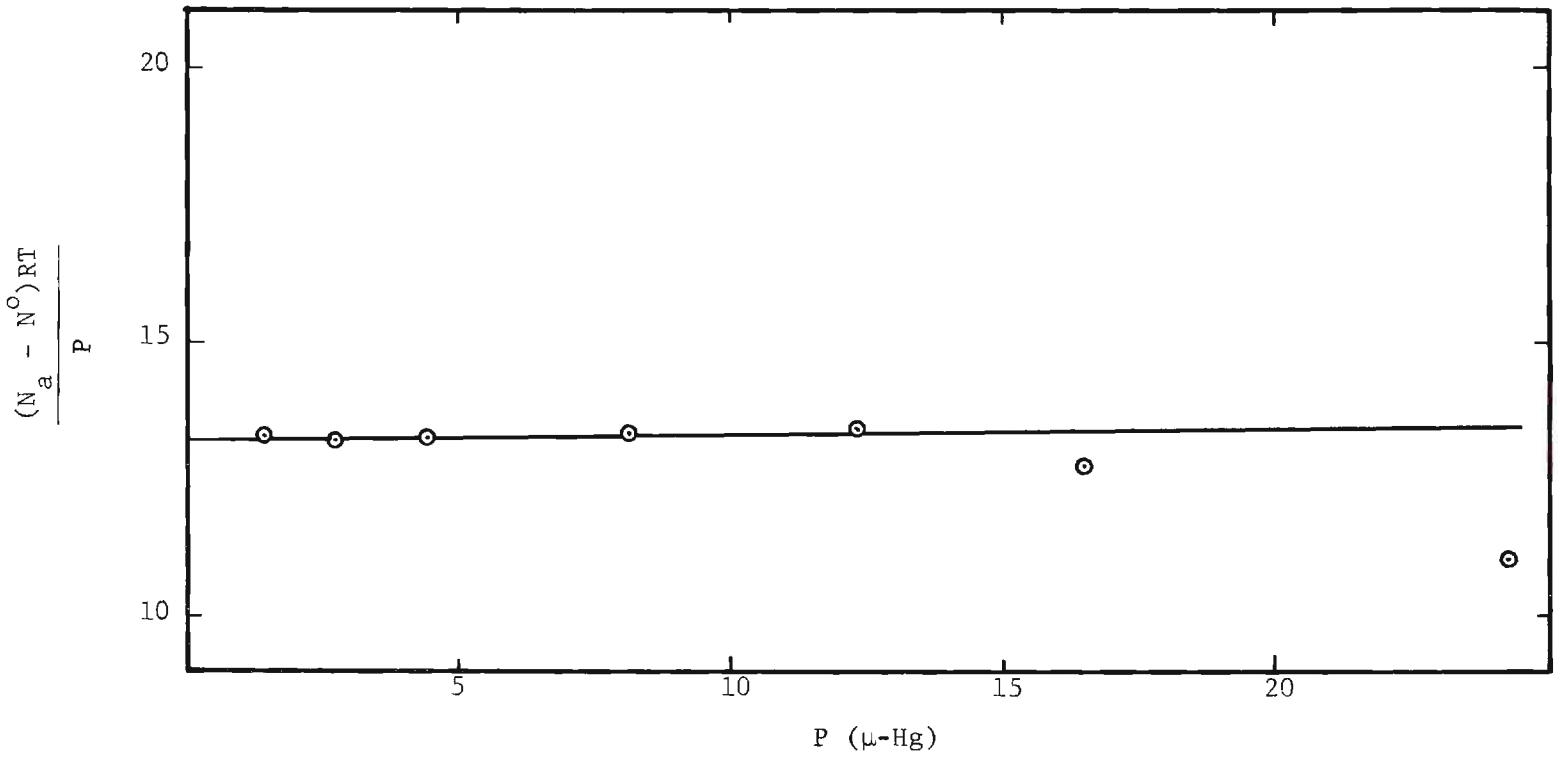

Figure 14. Virial Plot of the 91°K Isotherm Data After Correcting for the Non-Zero Intercept

The next step in the analysis was to relate the experimental values of $B_{2,S}$ to the parameters of the potential function given by equation (9). This was possible by noting that $\epsilon^*_{1,S}$, z_o, and A are independent of temperature and by making use of equation (13) which can be rearranged to give

$$\frac{B_{2,S}}{Az_o} = F\left(\frac{\epsilon}{kT}\right) \tag{51}$$

where $F\left(\frac{\epsilon}{kT}\right)$ is the summation in equation (13). If the correct value of $\epsilon = \epsilon^*_{1,S}$ is substituted into equation (51) and the experimental value of $B_{2,S}$ is divided by $F\left(\frac{\epsilon^*_{1,S}}{kT}\right)$ the result will be Az_o. Consequently, if the three experimental virial coefficients divided by $F\left(\frac{\epsilon}{kT}\right)$ are plotted against $\left(\frac{\epsilon}{k}\right)$, the three resulting curves will intersect at the point $\left(\frac{\epsilon^*_{1,S}}{k}, Az_o\right)$. This technique was used to determine values of $\epsilon^*_{1,S}$ and Az_o corresponding to the two sets of virial coefficients and the results are given in Table 6.

A, the surface area of the adsorbent, may be obtained from Az_o if z_o is known from some other source. An estimate of z_o was made by summing one-half the distance between nearest neighboring copper atoms in a cubic closest packed lattice[48] and one-half r_o for krypton[12]. This resulted in the value of 3.08 Å for z_o which was used in the calculations of A also listed in Table 6.

TABLE 6. Parameters from $B_{2,S}$ Analysis

Virial Coefficients	ϵ/k (deg. K)	Az_o (cm^3)	A (cm^2)
$B_{2,S}$	1907	1.73×10^{-7}	5.6
$B'_{2,S}$	1608	1.95×10^{-6}	63.4

The final step in the virial analysis was to determine the experimental values of $B_{3,S}$ and subsequently calculate $B_{2,D}$ and $\epsilon^*_{1,2}$. On the basis of the difficulties encountered in the determination of $B_{2,S}$, this further step could not be expected to produce any significant results, because as indicated by equation (47), $B_{3,S}$ depends on the value of $B_{2,S}$ and is also a stronger function of the pressure. Experimental values of $B_{3,S}$ were calculated, however, and indeed it was not possible to even determine the sign with certainty.

Significant Structures Analysis

The analysis outlined below generally follows a technique developed by McAlpin.[37] The procedure is to systematically extract values of the gas-surface interaction energy U_o or $\epsilon^*_{1,S}$ and ν, the characteristic frequency of the vibrations of the adsorbed atoms. The lateral interaction energy $\epsilon^*_{1,2}$ is then determined by adjusting it to obtain the best fit of the isotherm data. The relations used here apply onto to adsorbates which are atoms or spherical molecules.

The significant structures isotherm equation may be written

$$\ln P = \mu_g^o/kT - 2\theta \ln\left[\frac{B(6 - 5\theta)}{C}\right] + \frac{5\theta^2}{6 - 5\theta} - \ln\left(\frac{C}{\theta}\right) + 1 \qquad (52)$$

where

$$B = D(2\pi mkT/h^2)a_f e^{W/kT}$$

$$C = D(2\pi mkT/h^2)e\ a_m^o$$

$$D = \frac{\left(e^{-h\nu/2\ kT}\right)\epsilon^*_{1,S/kT}}{1 - e^{-h\nu/kT}}$$

$$\frac{\mu_g^o}{kT} = -\ln \frac{\left(2\pi m(kT)^{5/3}\right)^{3/2}}{h^2} .$$

Equation (52) includes the assumption that an adsorbed atom has six nearest neighbors at monolayer coverage, i.e., c = 6 in equation (32).

Equation (52) can be rearranged to give

$$\ln P + g(\theta) = -\ 2\theta \ln\left(\frac{B}{C}\right) - \mu_g^o/kT - \ln C \qquad (53)$$

where

$$g(\theta) = -\ln \theta - \frac{5\theta^2}{6 - 5\theta} + 2\theta \ln (6 - 5\theta) - 1 .$$

If $\ln P + g(\theta)$ is plotted against θ, the intercept of the resulting straight line will be $-\mu_g^o/kT - \ln C$. Since μ_g^o/kT can be evaluated exactly, $\ln C$ can be found from the intercept.

For an atomic adsorbate such as krypton

$$\ln C = 2 \ln T + \ln \left(\frac{k}{h\nu}\right)$$

$$+ \ln \left(\frac{2\pi m k a_m^o e}{h^2}\right) + \frac{\epsilon_{1,S}^*}{kT} \quad . \qquad (54)$$

Consequently, a plot of $\ln C - 2 \ln T$ against $\frac{1}{T}$ will give a straight line with $\frac{\epsilon_{1,S}^*}{k}$ as the slope and $\ln \left(\frac{k}{h\nu}\right) + \ln \left(\frac{2\pi m k T a_m^o e}{h^2}\right)$ as the intercept. Thus both $\epsilon_{1,S}^*$ and ν can be extracted from the isotherm data.

In the first attempt to analyze the data with the significant structures theory, all four isotherms were used to obtain values of $\epsilon_{1,S}^*$ and ν, and the 79°K isotherm was "best fit" to obtain $\epsilon_{1,2}^*$. This procedure led to a good fit for the 79°K isotherm, but the parameters obtained did not predict the higher temperature isotherms. A closer look at Figure 11 indicates a likely explanation. The 91°K isotherm exhibits an initial rapid increase in V_a with the pressure and then a region in which V_a is essentially constant with pressure. This behavior is characteristic of monolayer formation on a homogeneous surface. The coverage of the 79°K isotherm however always exhibits a pronounced pressure dependence. This indicates that multilayer formation is significant even as the first layer is filling. The form of the significant structures theory used here only applies to submonolayer adsorption consequently the 79°K isotherm should not be used in the fitting procedure. The parameters obtained from fitting the other isotherms should, however, predict the lower coverage region of the 79°K isotherm.

The three higher temperature isotherms were used to obtain $\epsilon^*_{1,S}$ and ν, and the 91°K isotherm was fit to obtain $\epsilon^*_{1,2}$. The resulting values along with the other parameter a^o_m required in the isotherm calculations are listed in Table 7. Figure 15 shows the resulting theoretical isotherms along with the experimental points. The correspondence is seen to be good. This formulation of the significant structures theory cannot be expected to correctly predict isotherms above coverages $\theta > 0.5$ to 0.6. The monolayer volume used in these calculations was 1.90×10^{-3} STP-cm^3, as indicated by the 91°K isotherm. This parameter is a scaling factor in the significant structures analysis and the value used does not appreciably affect the resulting interaction parameters.

Table 7. Parameters From Significant Structures Analysis of Copper-Krypton Isotherm Data

$\epsilon^*_{1,S}$	$\epsilon^*_{1,2}$	$\nu \times 10^{12}$	a^o_m
cal./mole	cal./mole	cyc./sec.	Å^2
3,490 ± 50	95 ± 15	4.62	19.5

The task of assigning uncertainties to parameters resulting from a significant structures analysis is rather complex and has received some attention.[37] The uncertainties listed above are approximate values based on an assumed uncertainty of 10 percent in the values of N_a which are most significant in the determination of the parameter. The uncertainties represent the accuracy of the parameters only to the extent

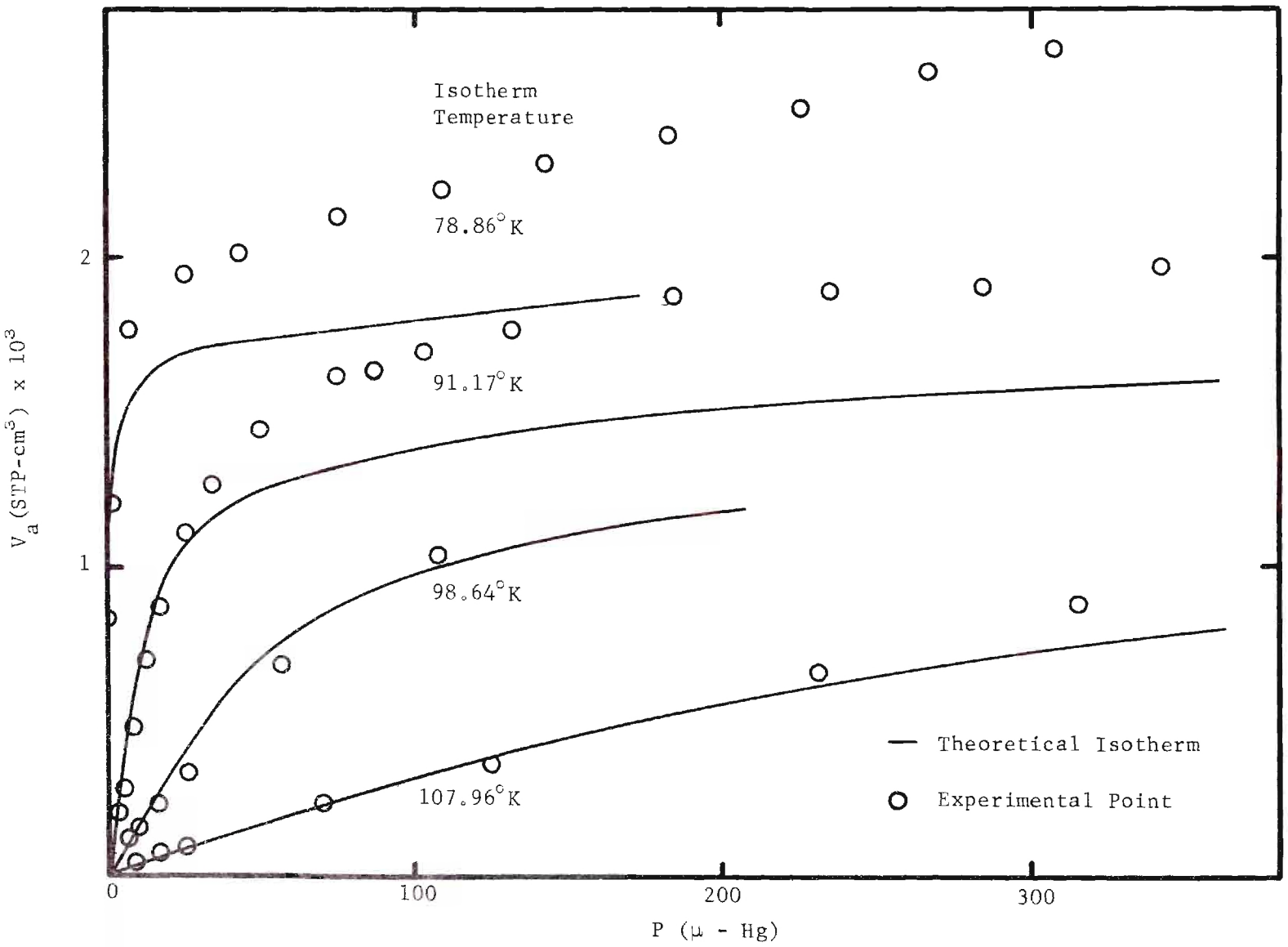

Figure 15. Significant Structures Isotherms

that the significant structures theory is accepted as being a true model of the copper-krypton system.

Discussion of the Results

Virial Analysis

The virial equation of state predicts that no gas will be adsorbed at zero pressure and that the initial portion of the isotherm, the so-called Henry's Law region, will be characterized by N_a being an almost linear function of the pressure. The isotherms obtained in the course of these experiments did not display either of these characteristics, consequently, the virial equation could not be used in a straight forward way to analyze the data.

The initial set of virial coefficients obtained in this chapter represent an analysis which considers only the first few low coverage points of the isotherms. For the 91°K isotherm (see Figure 13) these are the points which lie along that portion of the isotherm which is curving in toward zero coverage. This portion of the isotherm is decidedly nonlinear and too little data are available to establish the uncertainty in these coefficients. The very low value of the area obtained from the analysis, however, clearly indicates that the treatment is unrealistic. This may be the result of erroneous values of the virial coefficients or a poor choice of a model function to represent the gas-solid interactions.

As illustrated in Figure 13, the amount of gas adsorbed in a linear function of the pressure over a significant range of the 91°K isotherm. This is also true for the other two isotherms treated with

the virial analysis. These linear regions are pseudo-Henry's Law regions because N_a extrapolates to a non-zero intercept. One model[47] which accounts for this behavior is as follows: The surface is considered to be divided into two areas defined by different gas-solid interaction parameters, $\epsilon^*_{1,S}$. The area with the higher interaction potential represents only a small fraction of the total surface area of the adsorbent. As the adsorption process proceeds from zero coverage, the adsorbate is selectively concentrated over the area of higher $\epsilon^*_{1,S}$. This continues until the density above this area becomes sufficiently high to prevent it from making any further significant contribution to the total adsorption. At this point the adsorption can appear to obey Henry's Law if the density above the smaller $\epsilon^*_{1,S}$ area is still sufficiently low for Henry's Law to apply in this region. Consequently, the virial coefficients, $B'_{2,S}$, obtained by considering the isotherms to have a non-zero coverage at zero pressure are primarily determined by the interactions over the major fraction of the surface. In this case one would like to speculate that this is the copper face of interest, i.e., the (1,1,1) plane. In fact, the value of $\epsilon^*_{1,S}$ obtained from the analyses results from an averaging over all of the gas-surface interaction energies in the system, and consequently, can only be considered an estimate of the krypton-copper (1,1,1) interaction energy.

The virial treatment does lead to one very interesting qualitative conclusion. According to the virial theory, the regions of near linearity of the isotherms represent states of the adsorbate where only gas-solid interactions are significant. In the isotherms reported here these regions extend to coverages of $\theta = 0.3$ to 0.4. This result is interesting

because interactions within the adsorbed phase become important at much lower coverages over most homogeneous adsorbents such as graphite. This leads to the conclusion that $\epsilon^*_{1,2}$ is unusually small for the copper-krypton system. The significant structures analysis yields quantitative evidence of this

Significant Structures Analysis

The value of $\epsilon^*_{1,S}$ resulting from the significant structures analysis is in excellent agreement with the value found by McAlpin[1] for krypton interacting with the (1,1,1) face of copper thus establishing this parameter with a degree of certainty. The really interesting result of the analysis is the very low value found for $\epsilon^*_{1,2}/k = 48^\circ K$. This parameter has a value of $171^\circ K$ for krypton gas, implying a 70 percent reduction in the minimum in the krypton-krypton interaction potential in the presence of the copper surface. This result would seem to imply that three body effects such as those treated by Sinanoğlu and Pitzer and by McLachlan are of great importance on metallic surfaces.

CHAPTER V

CONCLUSIONS AND RECOMMENDATIONS

Conclusions

Four isotherms of krypton adsorbed on the (1,1,1) face of copper have resulted from this study. These isotherms have led to the following conclusions about the copper-krypton system:

(a) $\epsilon^*_{1,S}$, the copper-krypton interaction parameter, has a value of 3490 cal/mole.

(b) $\epsilon^*_{1,2}$, the krypton-krypton interaction parameter has a value of 95 cal/mole in the presence of the copper surface as compared to 340 cal/mole[12] in the gas phase.

It was found that the virial equation as it is normally applied was of little value in characterizing this system. This was probably due to the existence of some heterogeneity on the copper surface. It would appear that this same problem would plague any similar analysis involving a surface with even a minute degree of heterogeneity.

The significant structures theory did predict the isotherm behavior quite well and the parameters obtained from it were considered to be reliable. The results of the virial analysis were in qualitative agreement with these results also.

Finally, it is felt that this type of experiment does provide a sensitive tool for the study of dispersion interactions and other "low energy" inter-atomic forces.

Recommendations

It is felt that two changes in the experimental apparatus are desirable. First, the type 304 stainless steel tubing leading to the sample cell should be replaced by nickel or some other type of metal tubing which is not oxidized by water vapor at temperatures below 700°C. Second, the oil diffusion pump should be replaced by an ion pump with a capacity of approximately 40.1 per sec. This would preclude any contamination of the sample by oil from the mechanical or diffusion pump and would lower the ultimate pressure in the system due to the increased pumping speed of the ion pump.

Another area requiring further improvement is the preparation and characterization of the surfaces of the copper single crystals. X-ray analysis provides a means of determining the orientation of the crystal lattice with respect to the faces but it is more important to know what the chemical composition and structure of the crystals are at the interface. Tools have recently become available which can provide this information. Low energy electron diffraction (LEED) can establish the arrangement of the atoms of the solid at or very near the interface and Auger electron spectroscopy (AES) can determine what elements are present in this region. A preliminary Auger analysis was carried out on one of the crystals used in this study and the results are given in Appendix B. By properly applying these techniques it should be possible to obtain a well characterized metallic surface for adsorption studies.

An important extension of this study would include the measurement of isotherms on copper crystals with other orientations at their broad faces. The seed crystals required for these studies are available, and

with the apparatus which was developed for this study it should be possible to obtain additional data with a reasonable expenditure of time and funds.

Finally, it would be interesting to obtain additional low temperature data and analyze it with a multilayer model such as that of Newsome[2] which yields the adsorbate-adsorbate interaction energy between layers. Both the theories of Sinanoğlu and Pitzer and McLachlan predict an increase over the gas phase value in the adsorbate-adsorbate interaction energy between the first and second layers. Such a study might provide additional confirmation of these theories.

APPENDIX A

Isotherm Data

Table 8. Isotherm Data at 78.86°K

	V_{ads} (STP - cm^3) × 10^3	
P_{eci} (μ-Hg)	Copper Plus Cell	Copper Only
0.05	0.816	0.156
0.23	1.499	0.448
0.49	2.185	0.825
0.99	2.918	1.196
7.08	4.962	1.777
25.06	6.416	1.950
42.98	7.139	2.020
74.87	7.931	2.136
109.28	8.488	2.218
143.55	8.963	2.308
183.05	9.381	2.396
224.70	9.764	2.479
265.62	10.144	2.584
308.46	10.463	2.668
349.27	10.796	2.796
385.60	11.028	2.853
459.51	11.498	2.998
583.15	12.193	3.198

Table 9. Isotherm Data at 91.17°K

	V_{ads} (STP - cm^3) x 10^3		Maximum Error Copper Only
P_{eci} (μ-Hg)	Copper Plus Cell	Copper Only	(STP - cm^3) x 10^3
0.61	0.509	0.062	0.033
1.41	0.722	0.124	0.045
2.75	0.950	0.193	0.063
4.41	1.175	0.280	0.084
8.08	1.572	0.475	0.086
12.29	1.968	0.700	0.108
16.41	2.281	0.872	0.119
24.25	2.753	1.105	0.167
32.94	3.128	1.268	0.209
48.41	3.602	1.442	0.261
74.66	4.168	1.618	0.338
86.13	4.320	1.632	0.483
102.18	4.547	1.695	0.510
131.15	4.862	1.765	0.556
183.42	5.311	1.880	0.642
233.73	5.635	1.895	0.748
283.36	5.889	1.910	0.864
340.37	6.181	1.980	1.006
393.62	6.410	2.045	1.141
529.33	6.854	2.170	1.426
664.94	7.198	2.338	1.758
751.60	7.275	2.310	2.020

Table 10. Isotherm Data at 98.64°K

	V_{ads} (STP - cm^3) × 10^3		Maximum Error Copper Only
P_{eci} (μ-Hg)	Copper Plus Cell	Copper Only	(STP - cm^3) × 10^3
0.70	0.270	0.014	0.019
1.45	0.359	0.029	0.026
2.38	0.438	0.045	0.035
4.15	0.551	0.073	0.041
7.22	0.689	0.113	0.056
10.69	0.818	0.154	0.069
16.53	1.001	0.223	0.089
26.37	1.264	0.325	0.113
56.34	1.930	0.660	0.170
82.95	2.379	0.895	0.221
107.91	2.701	1.035	0.261
135.20	2.983	1.150	0.316
163.01	3.236		
192.54	3.462		
250.76	3.804		
307.67	4.096		
367.60	4.340		
423.40	4.549		
477.24	4.724		
534.12	4.863		
638.11	5.062		
723.64	5.240		

Table 11. Isotherm Data at 107.96°K

	V_{ads} (STP - cm^3) x 10^3		Maximum Error Copper Only
P_{eci} (μ-Hg)	Copper Plus Cell	Copper Only	(STP - cm^3) x 10^3
3.59	0.237	0.013	0.044
9.63	0.347	0.041	0.063
16.34	0.436	0.066	0.079
25.82	0.538	0.092	0.096
69.97	0.903	0.240	0.168
124.83	1.257	0.365	0.251
230.74	1.845	0.660	0.367
315.42	2.265	0.885	0.450
423.00	2.677	1.090	0.586
546.02	3.063	1.275	0.598
694.12	3.383	1.395	0.848

Table 12. Sample Cell Isotherm at 78.84°K

P_{eci} (μ-Hg)	V_{ads} (STP - cm^3) × 10^3
0.01	0.541
0.15	0.922
0.38	1.240
0.75	1.570
1.34	1.909
4.49	2.794
9.85	3.494
27.48	4.576
55.67	5.427
88.02	6.006
123.81	6.436
158.75	6.786
204.59	7.150
255.60	7.492
313.31	7.813
386.33	8.174
464.53	8.526
558.29	8.921
652.53	9.244

Table 13. Sample Cell Isotherm at 91.17°K

P_{eci} (μ-Hg)	V_{ads} (STP - cm^3) × 10^3
0.17	0.289
0.81	0.494
1.70	0.641
3.10	0.787
4.70	0.912
8.51	1.115
12.39	1.276
16.30	1.416
25.68	1.682
33.68	1.876
48.48	2.162
72.41	2.516
99.26	2.822
150.87	3.250
245.90	3.792
339.69	4.200
445.75	4.506
582.04	4.706
680.59	4.881
772.48	4.986
823.98	5.052

Table 14. Sample Cell Isotherm at 98.31°K

P_{eci} (μ-Hg)	V_{ads} (STP - cm^3) × 10^3
0.41	0.217
0.89	0.283
2.04	0.374
3.57	0.452
6.56	0.559
10.13	0.649
17.13	0.785
26.94	0.933
51.16	1.218
74.89	1.431
99.57	1.604
125.35	1.762

Table 15. Sample Cell Isotherm at 108.14°K

P_{eci} (μ-Hg)	V_{ads} (STP - cm^3) × 10^3
0.93	0.141
1.39	0.163
2.27	0.193
6.94	0.277
12.60	0.338
21.39	0.408
53.20	0.588
99.96	0.784
204.34	1.113
291.49	1.332
401.98	1.563
539.13	1.774
665.86	1.928
710.35	2.014

APPENDIX B

CHARACTERIZATION OF THE COPPER CRYSTATS

Bulk Structure

The orientation of the crystal lattice with respect to the broad faces was determined by a standard x-ray diffraction orientation technique for a number of the crystats and found to be within 3 degrees of the (1,1,1) plane. The slight crowning of the faces of the crystals resulting from the polishing procedure introduced some uncertainty into the determination.

Topography

The equipment required for low energy electron diffraction characterization of the surface was not available, consequently, the arrangement of the copper cores at the surface of the crystals could not be determined. Until this experiment is performed it can only be assumed that the bulk lattice extends to the surface of the crystals. This information will become more valuable when similar adsorption experiments are performed on other faces of copper single crystals.

Figure 16 is a photograph of the copper crystals used in these experiments. There is some macroscopic roughness, particularly at the upper end when electrical contact had to be established during the polishing procedure, but the majority of the surface area appears to be quite smooth.

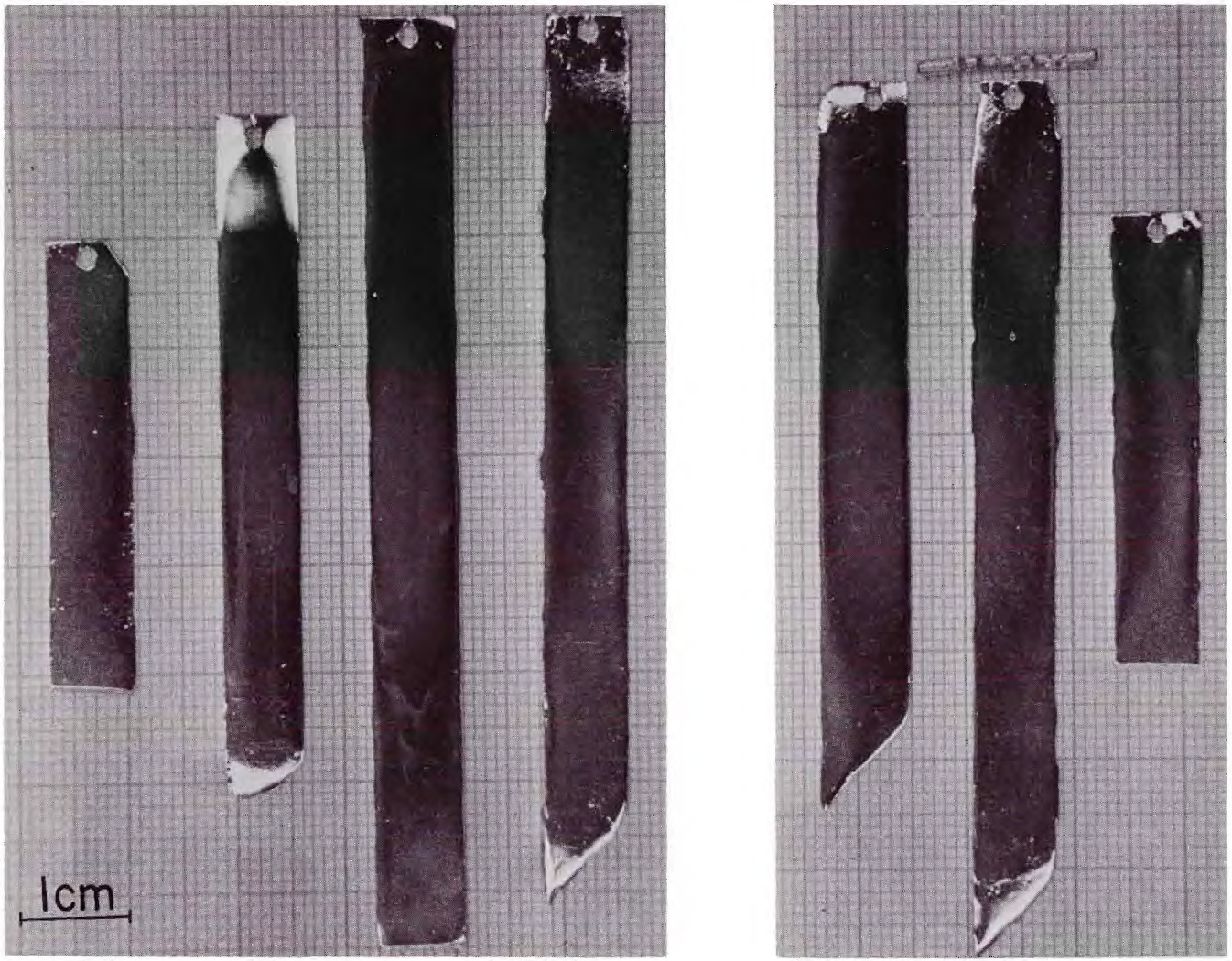

Figure 16. Copper Crystals

Figure 17 is a scanning electron micrograph of an area near one of the surface pits. The area to the lower left of the figure is characteristic of the smooth portions of the surface and is structureless at this magnification.

Chemical Composition of the Interfacial Layers

An Auger electron spectrometer was used to determine the elements present in the first two to five layers of atoms at the surface of one of the crystats. A review of the applications of this instrument to surface analysis has recently been published by Chang.[49] Some interesting information was obtained during the course of these experiments and it is summarized below.

In the initial experiment, one of the crystats, which had been stored in a protective but open container since the conclusion of the adsorption measurements some three months earlier, was placed in the spectrometer and the system was pumped to the range of 10^{-9} torr. A spectrum was obtained which indicated the presence of oxygen, nitrogen, carbon, and copper in the first few surface layers.

The crystal was then heated indirectly by electron bombardment of its holder. Heating for one half hour at $750^{o}C$ was found to completely eliminate any trace of nitrogen and oxygen from the energy spectrum. The carbon peak, however, was unaffected by heating.

Next, the surface of the crystal was bombarded with argon ions; a process, reverse sputtering, which tends to slowly erode the atoms at the surface of the sold. Sputtering dramatically reduced the indication of carbon and increased that of copper in the Auger spectrum. This would seem to indicate that the carbon present was

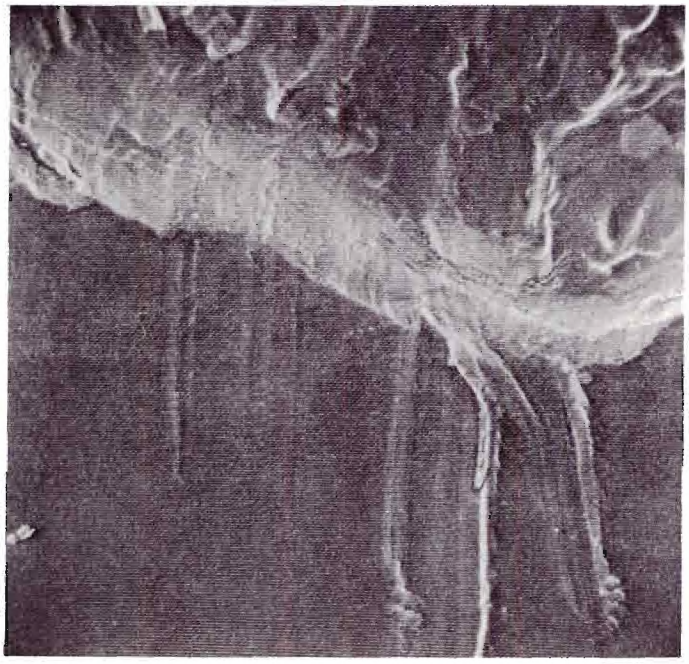

Figure 17. Scanning Electron Micrograph of Copper Surface Near Pit. (20 KV Beam at 45° Tilt, 20,000 x)

largely confined to the surface of the crystal. The shape of the carbon Auger peak was characteristic of graphite,[50] consequently, the carbon may have been present as a surface graphitic layer covering some fraction of the surface.

Finally, the spectrometer was filled with room air for approximately a week and then returned to ultra-high vacuum conditions. The Auger spectrum indicated the presence of oxygen and nitrogen and again these elements were removed by heating. The spectrum, however, indicated no change in the post-sputtering level of carbon.

The Auger experiments lead to the following conclusions:

(a) It may be possible to remove any oxygen at the surface of the copper crystals simply by heating to 750°C thus eliminating the need for the hydrogen reduction treatment. This is important for two reasons: (a) The reduction treatment forms water vapor which is difficult to remove from the vacuum system and (b) Hydrogen dissolves in the nickel sample cell and then revaporizes when the hydrogen treatment is concluded producing a virtual leak during the adsorption measurements.

(b) The crystals were contaminated with carbon at some point in the experiment. With the aid of the Auger spectrometer it should be possible to pinpoint the source of this contamination and eliminate it. The application of the Auger spectrometer to this task is greatly simplified because exposure to the atmosphere does not appear to lead to carbon contamination of the copper surface.

BIBLIOGRAPHY

1. D. M. Young, and A. D. Crowell, "Physical Adsorption of Gases," Butterworth, London (1962).

2. D. S. Newsome, Ph.D. Thesis, Georgia Institute of Technology (1972).

3. R. Wolfe and J. R. Sams, J. Phys. Chem., 69, 1129 (1965).

4. S. Brunauer, "The Adsorption of Gases and Vapors," Vol. I, Princeton University Press (1945).

5. G. D. Halsey, Jr. and C. M. Greenlief, Annual Review of Physical Chemistry, 21, 129 (1970).

6. T. L. Hill, Advan. Catalysis, 4, 211 (1952).

7. W. A. Steele, in J. T. G. Overbeek, W. Prins, and A. C. Zettlemoyer, Eds., "Advan. in Colloid and Interface Science," Vol. I, Elsevier Publishing Co., Amsterdam (1967).

8. E. A. Flood, Ed., "The Solid-Gas Interface," Vols. I and II, Marcel Dekker, New York (1967).

9. R. A. Pierotti and H. E. Thomas in Egon Matijevic, Ed., "Surface and Colloid Science," Vol. IV, Wiley-Interscience, New York (1971).

10. J. M. Honig, Ann. N. Y. Acad. Sci., 58, 741 (1954).

11. F. London, Z. Physik., 63, 245 (1930).

12. J. O. Hirschfelder, C. F. Curtis, and R. B. Bird, "Molecular Theory of Gases and Liquids," Wiley, New York (1954).

13. A. Müller, Proc. Roy. Soc. (London), A154, 624 (1936).

14. N. N. Avgul, A. A. Isirikyan, A. V. Kiselev, L. A. Lygina, and D. P. Poshkus, Izvest. Akad. Nauk, S. S. S. R., Otdel. Khim. Nauk., 1314 (1957)

15. W. G. Pollard, Phys. Rev., 60, 578 (1941).

16. T. L. Hill, J. Chem. Phys., 16, 181 (1948).

17. W. J. C. Orr, Trans. Faraday Soc., 35, 1247 (1939).

18. D. M. Young, Trans. Faraday Soc., 47, 1228 (1951).

19. A. D. Crowell and D. M. Young, Trans. Faraday Soc., 49, 1080 (1953).

20. J. E. Lennard-Jones, Trans. Faraday Soc., 28, 333 (1932).

21. A. D. McLachlan, Mol. Phys., 7, 381 (1964).

22. T. N. Rhodin, Jr., Advan. Catalysis, 5, 40 (1963).

23. J. H. deBoer, Advan. Catalysis, 8, 29 (1956).

24. M. P. Freeman, J. Phys. Chem. 62, 729 (1958).

25. O. Sinanoğlu and K. S. Pitzer, J. Chem. Phys., 32, 1279 (1960).

26. E. A. Mason and T. H. Spurling, in J. S. Rolinson, Ed., "The International Encyclopedia of Physical Chemistry and Chemical Physics," The Virial Equation of State, Pergamon Press, New York (1969).

27. W. A. Steele and G. D. Halsey, J. Chem. Phys., 22, 979 (1954).

28. T. L. Hill, "Statistical Mechanics," McGraw-Hill, New York, 425 (1965).

29. R. A. Pierotti, Chemical Physics Letters, 2, 385 (1968).

30. W. G. McMillan and J. E. Mayer, J. Chem. Phys., 13, 276 (1945).

31. J. A. Barker and D. H. Everett, Trans. Faraday Soc., 58, 1608 (1962).

32. J. R. Sams, G. Constabaris, and G. D. Halsey, J. Phys. Chem., 64, 1689 (1960).

33. H. Eyring, T. Ree, and N. Hirai, Proc. Natl. Acad. Sci. U.S., 44, 683 (1958).

34. J. J. McAlpin and R. A. Pierotti, J. Chem. Phys., 41, 68 (1964).

35. J. E. Lennard-Jones and A. F. Devonshire, Proc. Roy. Soc. (London), A163, 53 (1937).

36. T. L. Hill, "Introduction to Statistical Thermodynamics," Addison-Wesley, Reading (1960).

37. J. J. McAlpin, Ph.D. Thesis, Georgia Institute of Technology (1966).

38. B. R. Brymner and W. Steckelmacher, J. Scientific Instruments, 36, 278 (1959).

39. L. Bewilogua and E. Müller, Cryogenics, 2, 178 (1961).

40. Grinnell Corporation, Catalogue WFF-67, Providence, R. I., 93 (1967).

41. B. B. Fisher and W. G. McMillan, J. Phys. Chem., 62, 494 (1958).

42. Beaumont, Chihara, and Morrison, Proc. Phys. Soc. (London), 78, 1462 (1961).

43. W. G. Bronbacher, D. P. Johnson, and J. L. Cross, NBS Monograph 8 (1960).

44. Communication from R. Wolf, President, MKS Instruments, Inc., Burlington, Mass.

45. N. G. Utterback and J. Griffith, The Review of Scientific Instruments, 37 (1966).

46. G. A. Miller, J. Phys. Chem., 67, 1359 (1963).

47. H. E. Thomas, Ph.D. Thesis, University of Brystol (1969).

48. L. Pauling, "The Nature of the Chemical Bond," Cornell University Press, Ithaca, pg. 410 (1960).

49. C. C. Chang, Surface Science, 25, 53 (1971).

50. T. W. Haas, J. T. Grant, and G. J. Dooley III, J. Appl. Phys., 43, 1853 (1972).

VITA

John Lewis Carden, Jr. was born in Nashville, Tennessee, the son of Cecelia Johnson and John Lewis Carden. He was reared in Nashville and was graduated from Madison High School in June 1961. He entered the freshman class at Vanderbilt University in September 1961 as the Duncan Memorial Scholar and received the degree of Bachelor of Arts in chemistry in June 1965. He then entered the graduate division of the Georgia Institute of Technology to study for the Doctor of Philosophy in the School of Chemistry. During his graduate work he held a National Petroleum Research Fund fellowship, and served as a teaching and research assistant. The final year of his graduate study was spent in the Physical Sciences Division of the Georgia Institute of Technology Engineering Experiment Station.